A NOVEL VIBRATING-SAMPLE MAGNETOMETER USED TO MEASURE MAGNETIC HYSTERESIS OF ROCK AT LOW TEMPERATURE

GERALD M. ENGLISH

A NOVEL VIBRATING-SAMPLE MAGNETOMETER USED TO MEASURE MAGNETIC HYSTERESIS OF ROCK AT LOW TEMPERATURE

By

© GERALD M. ENGLISH B.Sc.

A thesis submitted to the School of Graduate
Studies in partial fulfilment of the
requirements for the degree of
Master of Science

Department of Earth Sciences (Geophysics)
Memorial University of Newfoundland
1995

St. John's Newfoundland

ISBN 0-612-06117-5

Abstract

A vibrating-sample magnetometer was constructed, calibrated and used to measure the magnetic hysteresis of rock samples. The magnetometer was designed around a large electromagnet capable of producing fields of approximately 3600 Oe (360 mT). Between the poles of this magnet, pick-up coils and a liquid nitrogen bath surrounded a sample port assembly in which the sample could be vibrated. The sample port assembly contained a heating element that allowed the sample temperature to be varied from room temperature to 98 K (-175°C). A novel method was used to vibrate the large (5 gram) rock samples. The sample was mounted off-axis on a rotating shaft in a way that kept the sample's orientation in the applied field from changing while the sample moved uniformly in a circle of 2 mm radius 29.2 times a second. This induced a 29.2 Hz sinusoidal voltage in the pick-up coils proportional to the magnetization of the sample. Cycling the magnetic field intensity allowed hysteresis loops to be automatically plotted.

Seven magnetite-bearing Precambrian dolerite dyke samples which had likely retained their original remanence direction for over a billion years were studied. Measurements of their magnetic hysteresis as a function of low temperature were used to investigate what mechanisms allowed them to retain such stable remanence.

The coercive force, H_C, of the samples decreased as a linear function of saturation magnetostriction on cooling. This suggests that internal stresses opposing

domain wall motion are mainly responsible for the ability of most of these rocks to retain stable remanence. The one clear exception was the specimen of highest coercive force (H_C = 487 Oe = 3.9×10^4 A/m) in which H_C hardly changed on cooling suggesting that remanence was carried by single-domain grains with shape anisotropy.

The ratio of saturation remanence to saturation magnetization J_R/J_S was found to change linearly with saturation magnetostriction and with coercive force on cooling. These linear relationships and that between coercive force and saturation magnetostriction were used to infer what proportion of the magnetite present was in the form of single-domain or pseudo-single-domain grains using the method of Hodych (1990). This method could not be applied to the sample of highest coercive force because its coercive force and saturation remanence did not change on cooling.

Reversible work, W_{rev}, done on descending from saturation to the remanence point in a hysteresis loop was measured as a function of low temperature. When W_{rev} was estimated by integrating to a constant magnetization rather than to a constant field, W_{rev} was found to decrease on cooling. However, this does not allow inference of what is controlling domain rotation in the samples.

TABLE OF CONTENTS

List of Tables

List of Figures

Note on Units

Throughout this thesis the data is presented using the Gaussian system of units followed by the SI equivalent units in brackets. This makes it easier to compare with earlier related work. The following list shows the magnetic terms, the symbols, the Gaussian and SI equivalent units, as well as the conversion factors by which data in Gaussian units must be multiplied to convert to SI units.

Magnetic Term	Symbol	Gaussian Unit	SI Unit	Conversion Factor
Magnetic field	H	Oersted	Tesla	$(x10^{-4})$
Magnetization	J	emu/cm^3	Tesla	$(x4\pi x10^{-4})$
Coercive force	H_C	Oersted	Ampere/metre	$(x10^3/4\pi)$
Saturation remanence	J_R	emu/cm^3	Tesla	$(x4\pi x10^{-4})$
Polycrystalline saturation magnetostriction	$\overline{\lambda}_S$	dimensionless	dimensionless	
Internal stress	σ	$dyne/cm^2$	Pascal	$(x10^{-1})$
Reversible work	W_{rev}	erg/cm^3	$Joule/metre^3$	$(x10^{-1})$
Self-demagnetizing factor	N	emu	Henry/metre	$(x1/4\pi x10^7)$

Acknowledgements

I wish to acknowledge with thanks the help received from the following people in the course of this work:

Dr. J.P. Hodych, under whose supervision these investigations were carried out, who offered encouragement and suggestions throughout this work.

Mr. T. Perks of the Technical Services Department, for the glass blowing required for the many Dewar flasks constructed and tested for the magnetometer.

Mr. H. Dye of the Technical Services Department, for machining and helping design the sample vibrator.

Mr. R. Pätzold, for his help in composing some of the diagrams.

CHAPTER 1

INTRODUCTION

1.1 Magnetic Hysteresis of Rock

In the study of rock magnetism, we seek to understand the magnetic properties of rocks and their magnetic minerals - primarily magnetite and hematite. This can help us explain the origin and reliability of the remanent magnetism of rocks used for palaeomagnetic studies. In the present study, low temperature variation of magnetic properties of magnetite-bearing Precambrian dolerites are studied to help understand why such rocks have been so successful in recording the ancient field of the Earth.

The magnetic properties that will be studied are those determined by measuring the hysteresis loop of the rock. If the magnetization (J) in a sample is measured as applied field (H) is increased and then decreased, magnetization is found to lag behind field leaving a remanent magnetization when field is removed. This phenomenon is called magnetic hysteresis. See Figure 1.1. The saturation magnetization (J_S) is reached by applying a magnetic field large enough that magnetization ceases to increase with field. When the saturating field is removed, the remanent magnetization left in the sample is termed saturation remanence (J_R). Applying field in the opposite direction to saturation remanence decreases total magnetization and the field required to reduce this total magnetization to zero is called coercive force (H_C). Hodych (1982a, 1982b, 1986b,

1990, 1991), has shown that measuring low temperature variation of H_c can help us determine the mechanism by which the magnetite retains natural remanence through geological time.

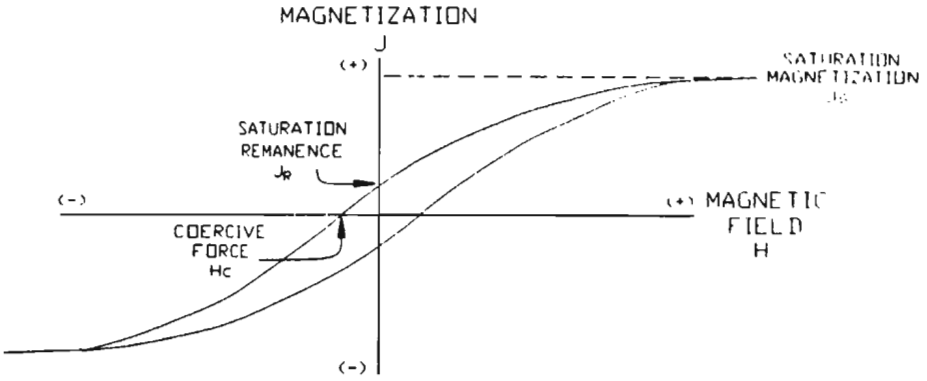

Figure 1.1: Magnetic hysteresis loop.

Generally, hysteresis loops measured for ferromagnetic substances are affected by self-demagnetizing fields. The magnetic field (H) applied to a multidomain grain induces a magnetization (J) whose magnetic poles apply a reverse self-demagnetizing field $H_D = NJ$. The self-demagnetizing factor (N) is generally assumed to be constant, depending only on the shape of the grain. Since the effective magnetic field inside the grain is H-NJ, many magnetic properties of rocks bearing multidomain magnetite are strongly influenced by N, making its determination important. J_S and H_c are unaffected

by self-demagnetizing fields, but J_R is reduced (Hodych, 1986a) causing the hysteresis loop to "shear" as shown in Figure 1.2.

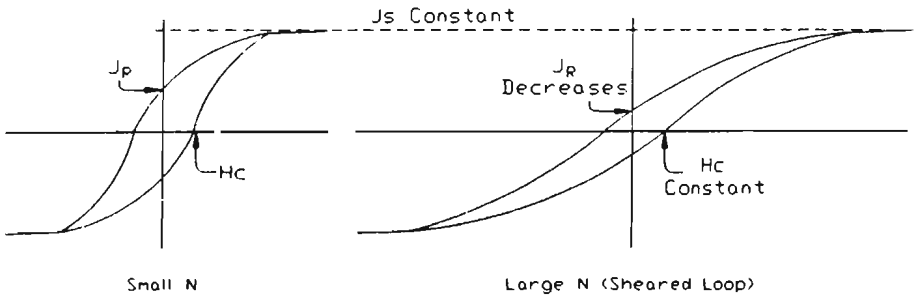

Figure 1.2: Hysteresis loops expected measuring along the axis of a long rod (left) and for a sphere (right) of the same multidomain material.

1.2 Magnetic Domain Theory

The size of the magnetic grain affects its magnetic behaviour. Very small grains may not be able to retain remanence at room temperature; these grains are termed superparamagnetic. Grains that are a little larger, are termed single-domain grains. They remain magnetized to saturation along an easy axis (an axis that is easy to magnetize) when field is reduced to zero. Magnetic field can only change their magnetization by rotating J_S from one easy axis to another. The saturation remanent magnetization of an assemblage of single-domain magnetite grains is a large fraction of saturation magnetization, and the coercive force tends to be of the order of 100 Oe (8.0×10^3 A/m)

or greater (Fuller, 1987).

Still larger grains of magnetite become spontaneously subdivided by walls into domains magnetized to saturation in opposite directions when field is reduced to zero. This reduces magnetostatic energy (the stored potential energy of free poles) at the expense of domain wall energy. The number of domains formed are such that the total energy in the sample, that is, the sum of magnetostatic and domain wall energies will be reduced to a minimum. Applying a field will cause domain walls to move, although the motion will be opposed by imperfections in the crystal. These imperfections allow the sample to retain a remanent magnetization when the field is removed. Rocks consisting of large multidomain grains of magnetite usually have lower coercive force and saturation remanence is a smaller fraction of saturation magnetization than in rocks with single-domain magnetite.

Sometimes grains are large enough to contain domain walls but still behave similarly to single-domain grains; these grains are termed pseudo-single-domain grains.

For palaeomagnetic work, single-domain grains or pseudo-single-domain grains are more desirable than larger multidomain grains because multidomain remanence is of lower coercivity and hence is more easily reset over geological time.

1.3 Shape Anisotropy

Magnetite grains are often easiest to magnetize along their longest axes because

self-demagnetizing fields are then lowest. In single-domain grains of magnetite, magnetostatic energy would usually be the dominant energy, controlling coercive force through shape anisotropy. For a randomly-oriented assemblage of elongated single-domain grains (with N_a and N_b being the self-demagnetizing factor along and transverse to the long axis of the grain respectively) coercive force should be given by (Stoner and Wolfarth, 1948);

$$H_C = 0.479\ (N_b - N_a)J_S$$

and,

$$J_R / J_S = ½$$

Since J_S for magnetite shows little change on cooling to liquid nitrogen temperature, elongated single-domain magnetite grains are expected to show little change in H_C on cooling.

1.4 Magnetocrystalline Anisotropy

Crystals are usually easier to magnetize along some crystallographic axes than others. For example, magnetite has cubic symmetry, and is easiest to magnetize along <111> and hardest to magnetize along <100>. The magnetocrystalline anisotropy energy, E_K, for a crystal like magnetite with cubic symmetry is given by, (Stewart, 1954);

$$E_K = K_0 + K_1 (\alpha_1^2\alpha_2^2 + \alpha_2^2\alpha_3^2 + \alpha_3^2\alpha_1^2) + K_2\alpha_1^2\alpha_2^2\alpha_3^2 + \ldots$$

where the α's are the direction cosines of the magnetization vector with respect to the cubic axes, and K_0, K_1, and K_2 are the magnetocrystalline anisotropy coefficients.

In single-domain magnetite, shape anisotropy would usually be expected to dominate over magnetocrystalline anisotropy (unless the grains were nearly spherical). Magnetocrystalline anisotropy could control coercive force in multidomain magnetite if for example domain wall motion was impeded by non-magnetic inclusions. In this case simplifying the theoretical result of Néel (1946) leads one to expect coercive force to vary in approximate proportion to magnetocrystalline anisotropy, as given by;

$$H_C \propto |K_1| / J_S$$

On cooling, K_1 for magnetite decreases to zero at approximately 140 K (T_K, the "isotropic" point) and then changes sign. At approximately 120 K (T_V, the Verwey transformation) magnetite transforms from cubic to orthorhombic with a great increase in magnetocrystalline anisotropy. Hence, H_C controlled by non-magnetic inclusions impeding domain wall motion should drop to near zero on cooling to T_K and then increase sharply on cooling to T_V.

1.5 Stress-induced Anisotropy

Magnetostriction is the fractional change in a sample's dimensions with a change in its magnetization. Conversely, changing a sample's dimensions by applying stress will change its magnetization making some axes easier to magnetize than others. This stress-induced anisotropy in the case of a cubic crystal such as magnetite can be described by stress-induced anisotropy energy, $E_{\lambda\sigma}$ given by (Carmichael, 1989);

$$E_{\lambda\sigma}=\frac{3}{2}\lambda_{100}\sigma\left(\sigma_1^2\beta_1^2+\alpha_2^2\beta_2^2+\alpha_3^2\beta_3^2\right)+3\lambda_{111}\sigma\left(\alpha_1\alpha_2\beta_1\beta_2+\alpha_2\alpha_3\beta_2\beta_3+\alpha_3\alpha_1\beta_3\beta_1\right)$$

where; σ is stress
α's are direction cosines of magnetization vector
ß's are direction cosines of stress, σ
λ_{100} is saturation magnetostriction along <100>
λ_{111} is saturation magnetostriction along <111>

For isotropic magnetostriction ($\lambda_{100}=\lambda_m=\lambda_s$) this simplifies to,

$$E_\sigma=\frac{3}{2}\lambda_s\sigma\sin^2\phi$$

where ϕ is the angle between the direction of the stress and the direction of the magnetization. For magnetite, magnetostriction is far from isotropic, but the polycrystalline saturation magnetostriction $\overline{\lambda} = 0.4\lambda_{100} + 0.6\lambda_{111}$ is often used in place

of λ_s in the above expression.

In multidomain grains, internal stresses (σ) may control coercive force by impeding domain wall motion. Simplifying (Néel's, 1946) theoretical prediction and assuming isotropic magnetostriction, leads one to expect coercive force to vary in approximate proportion to $\overline{\lambda}_s$ as given by;

$$H_c \propto \sigma \, \overline{\lambda}_s / J_s$$

On cooling, $\overline{\lambda}_s$ for magnetite gradually decreases until T_v is reached. Hence, H_c controlled by internal stresses impeding domain wall motion should decrease on cooling to T_v.

1.6 Objectives

The purpose of this study was to design and construct a vibrating-sample magnetometer to measure the magnetic properties of magnetite contained in rock as the rock is cooled from room temperature to near liquid nitrogen temperature 77 K (-196°C) and to interpret the results.

The vibrating-sample magnetometer constructed for this thesis was designed to be simple but robust so that it could vibrate a large rock sample (1-2 cm^3) at an amplitude that remains constant as temperature is varied to liquid nitrogen temperature.

Details of the new magnetometer are given in the next chapter.

This magnetometer was used to measure hysteresis as a function of low temperature to obtain evidence as to the domain state and controls on coercive force of the magnetite in rock samples of high coercive force. Morrish and Watt (1958) measured the variation in coercive force of various grain sizes of crushed magnetite on cooling to liquid nitrogen temperature. For these multidomain magnetites, they found that coercive force decreased on cooling until near the Verwey transition (~120 K) and they assumed that this decrease was due to the decrease in K_1 on cooling. For elongated single-domain magnetite powder, they found coercive force to show relatively little variation on cooling which was consistent with J_S control of coercive force through shape anisotropy.

The effect of cooling to liquid nitrogen temperature on the hysteresis loops of rocks containing magnetite or titanomagnetite was measured by Radhakrishnamurty et al., 1972, 1978, Deutsch and Pätzold, 1976 and Murthy et al., 1976. These results were then interpreted to suggest the domain state of the magnetite or titanomagnetite in the rocks.

Hodych (1982a) showed that H_C in the experiments of Morrish and Watt (1958) on multidomain magnetites varied in proportion to $\overline{\lambda}_S$ (Figure 1.3) rather than K_1 suggesting that coercive force of these samples was controlled magnetostrictively through internal stresses opposing domain wall motion. Hodych (1982a, 1986b, 1990) showed that H_C of magnetite-bearing rocks often varies in approximate proportion to $\overline{\lambda}_S$ rather than J_S or K_1 on cooling. This suggests that internal stresses opposing domain wall

motion are an important control on remanence retention in magnetite-bearing rocks. Xu and Merrill (1990) supported this view in their theoretical study of how internal stresses associated with dislocations impede domain wall motion in magnetite.

Worm and Markert (1987) made hysteresis loop measurements on titanomagnetites that were precipitated in artificial silicate glass and likely have high internal stresses. For a few of their samples, hysteresis loops were measured at temperatures from 4 to 700 K. On comparing the variation of coercive force with temperature with the variation of J_S, K_1 and λ_S with temperature, they concluded that these titanomagnetites owe their coercivity to stress-induced anisotropy rather than shape anisotropy or magnetocrystalline anisotropy.

On the other hand, Schmidbauer and Schembera (1987) prepared synthetic magnetite samples with very low internal stresses. They measured magnetic hysteresis loops as a function of decreasing temperature for these samples and concluded that coercive force varies like the magnetocrystalline anisotropy constant on cooling.

Argyle and Dunlop (1990) also used magnetites that likely had very low internal stresses (being hydrothermally grown). They measured hysteresis loops as a function of temperature, finding that coercive force changed linearly with K_1/J_S between 250 and 376 K, implying magnetocrystalline control.

It seems likely that internal stresses are high in most natural magnetites and that magnetostrictive control of H_C may be common except for rocks of very high coercive force where shape anisotropy may well dominate. One aim of the present thesis was to

extend the methods of Hodych (1982a, 1986b, 1990) to higher coercive force specimens. This required replacing the original air-cored coil used by Hodych with an electromagnet capable of producing higher fields and designing a vibrating-sample magnetometer to use with the electromagnet.

Appel (1987) estimated internal stress magnitude in titanomagnetite in rock using reversible work recovered between saturation and the remanence point of the hysteresis loop. He assumed that internal stresses could be estimated using the relation $\sigma = W_{rev}/\lambda_S$. Hodych (1990) tried applying this method to magnetite in rocks, but found that it did not seem to be reliable because reversible work did not decrease in proportion to λ_S on cooling. This method was tested further in this thesis.

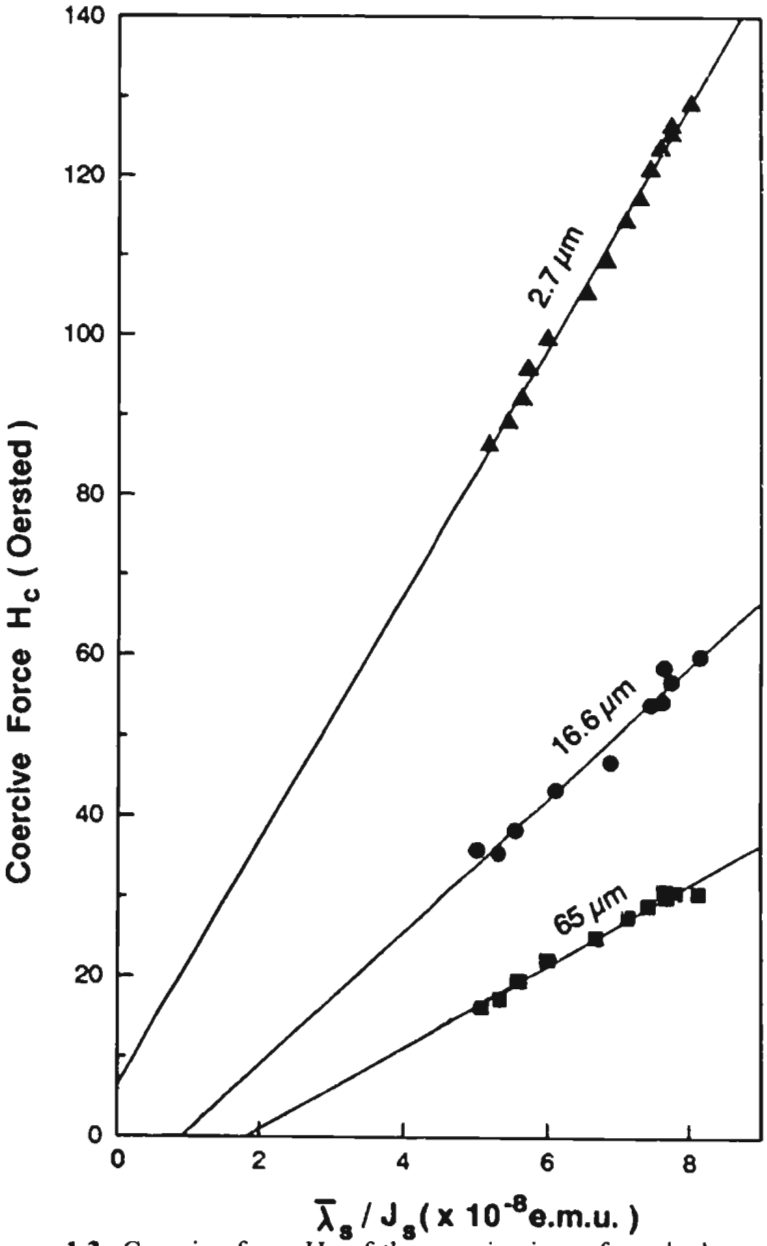

Figure 1.3: Coercive force H_c of three grain sizes of crushed natural magnetite measured between ~300 and ~130 K by Morrish and Watt (1958) plotted by Hodych (1982) versus polycrystalline saturation magnetostriction divided by saturation magnetization.

CHAPTER 2

THE VIBRATING-SAMPLE MAGNETOMETER

2.1 Introduction

The vibrating-sample magnetometer in one of its many forms, has long been the instrument commonly used by rock magnetists to determine the magnetic hysteresis parameters of rock samples. The hysteresis loop is measured and yields fundamental parameters such as the coercive force and the ratio of saturation remanence to saturation magnetization.

Within a vibrating-sample magnetometer, a magnetized sample is vibrated sinusoidally relative to a multi-turn pick-up coil. The changing magnetic flux through the pick-up coil induces a sinusoidal voltage in it which is proportional to the magnetization of the sample. The sample's magnetization is usually produced by a uniform magnetic field applied by a magnetizing coil or electromagnet. Measuring the magnetization of the sample by recording the voltage in the pick-up coils as the applied magnetic field is cycled allows hysteresis loops to be measured.

Blackett and Sutton (1956) were probably the first to describe a vibrating-sample magnetometer used for rock-magnetic measurements. Within their instrument, a disc of rock 2.3 cm in diameter and 0.5 cm thick was vibrated with an amplitude of 1.2 cm and a frequency of 30 Hz parallel to the disc axis and to the applied field of an

electromagnet. Magnetization within the sample was measured with two pick-up coils placed on either side of the sample and aligned co-axially to the sample. The output from these coils was amplified and read on a vibration galvanometer.

Foner (1959) used a loudspeaker drive to obtain a 90 Hz vibration with an amplitude of 0.1 to 1.0 mm. This system was designed to vibrate samples 6 mm in diameter or smaller perpendicular to the field of an electromagnet. A phase sensitive detector (also referred to as a lock-in amplifier) was used to acquire signals from the pick-up coils.

Kobayashi and Fuller (1967) described a system in which the sample was vibrated by an electric motor and a mechanical converter. This system was capable of vibrating samples of up to 25 grams longitudinally perpendicular to the field of an electromagnet at a frequency of 90 Hz with a vibration amplitude of 0.2 - 5.0 mm. The signal from the pick-up coils was processed using phase sensitive detection.

Creer, de Sa and O'Reilly (1967) constructed an instrument which used an air turbine to drive a scotch crank which in turn vibrated the sample longitudinally. They believed that this drive system would avoid the electromagnetic noise associated with motor and speaker drive systems. Their drive system, which was designed for use in a solenoid with axial pick-up coils, could vibrate a 1 gram sample at 70 Hz with a 1.2 cm stroke. However, the frequency of the air turbine drive was difficult to stabilize and the turbine was acoustically noisy. This led Hoye (1972) (*described in* Collinson (1983)) to replace the air turbine with a motor to vibrate the sample at 11 Hz with a 2.2 cm stroke.

Further modifications were made to this magnetometer by Tucker (1978) (*described in* Collinson (1983)) who replaced the axial pick-up coils by 5000 turn coils for use in the gap of an electromagnet. The coils were spaced 5 cm apart allowing room for a furnace and controlled atmosphere around the sample. A vibration amplitude of 1.5 cm and a frequency of 11 Hz was used. At room temperature, 2.5 cm rock samples could be used but for high temperature work, small (1 gram) samples were used.

Recently, Flanders (1988) described an alternating-gradient magnetometer. This vibrating-sample magnetometer claims to be 1000 times more sensitive than conventional designs, and capable of producing complete hysteresis loops over 10,000 Oe (1000 mT) in about 100 seconds. The sample is mounted on the end of a cantilevered rod that incorporates a piezoelectric element. The sample is magnetized by a variable DC field while simultaneously being subjected to a small alternating field gradient. The alternating field gradient exerts an alternating force on the sample, proportional to the magnetic moment of the sample. The resulting alternating deflection of the cantilevered rod is measured by the alternating voltage output of the piezoelectric element. This voltage is measured by a lock-in amplifier, giving an output proportional to the magnetic moment of the sample. The instrument has been used at temperatures ranging from 77 to 400 K. However, the sample was limited to approximately 1 gram or less.

The vibrating-sample magnetometer constructed for this thesis is of unique design. It was designed for measuring hysteresis loops of large rock specimens (~1.5 cm^3) in an electromagnet at various low temperatures. Figure 2.1 is a drawing which

identifies the components of the magnetometer and Figure 2.2 is a photograph of the magnetometer. The sample is moved uniformly around a circular path of 2 mm radius making 29.2 revolutions per second. This magnetometer is related to one built by Flanders (1967) in which a sample was also spun off-axis. However Flander's magnetometer was used to measure magnetic anisotropy, and could not measure hysteresis loops because the sample's orientation was continually changing in the applied field. In the magnetometer built for this thesis, the sample's orientation is kept constant relative to the field applied by a large electromagnet. The sample's motion relative to two fixed pick-up coils induces in the coils a 29.2 Hz sinusoidal signal which is proportional to the sample's magnetization. This signal is amplified and applied to the Y-axis of an X-Y plotter. Meanwhile, a signal proportional to the applied field is applied to the X-axis and a hysteresis loop is traced. Hysteresis loops can be traced for any temperature from 294 to 98 K using a temperature control assembly consisting of a liquid nitrogen reservoir, a resistive heating element and a specially-designed Dewar flask that surrounds the sample.

2.2 The Electromagnet

The magnetometer was designed to be used with a large electromagnet constructed by Dr. Bruce May in 1969 using the laminated iron core from a transformer. The core of this electromagnet shows no noticeable hysteresis in the field cycles used

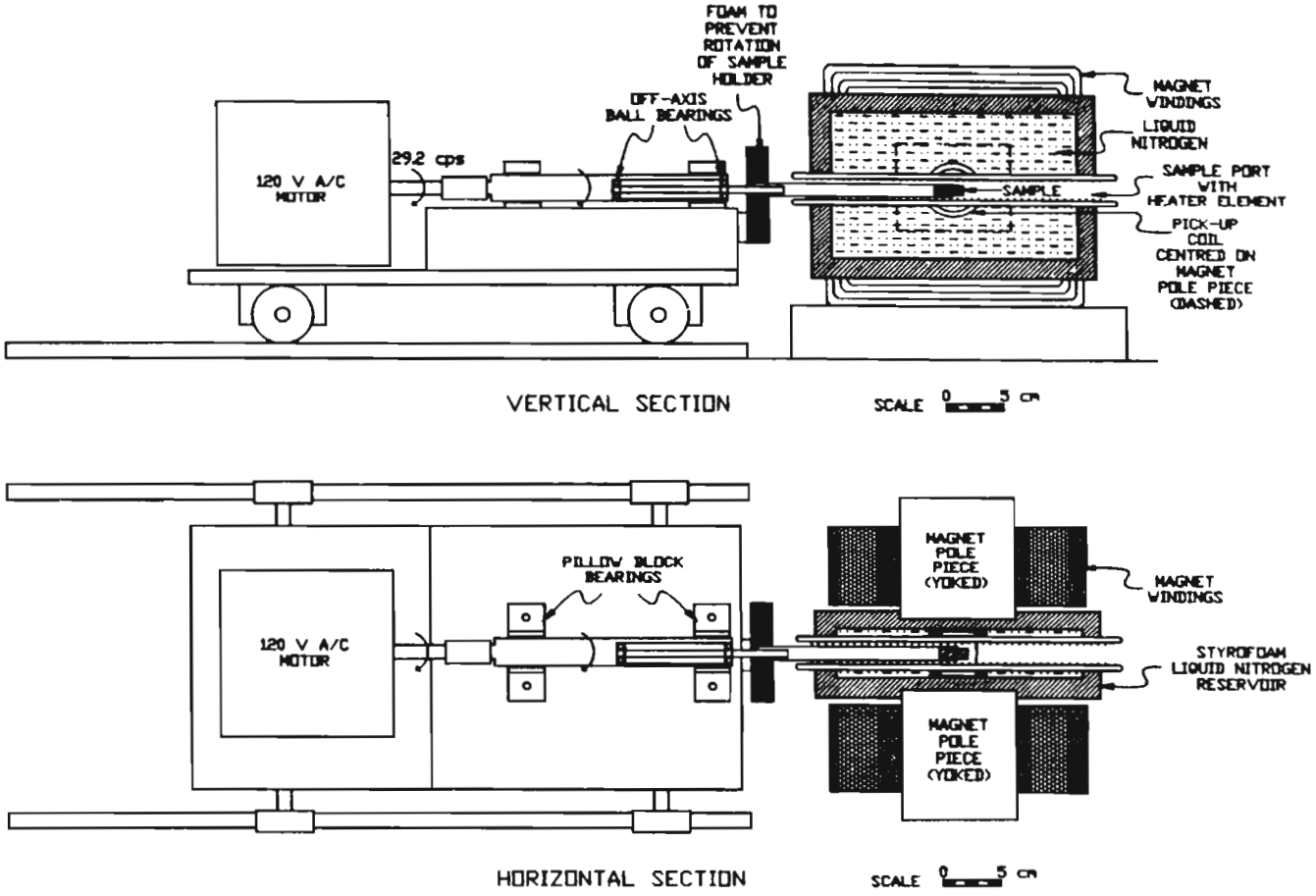

Figure 2.1: Drawing of the vibrating-sample magnetometer.

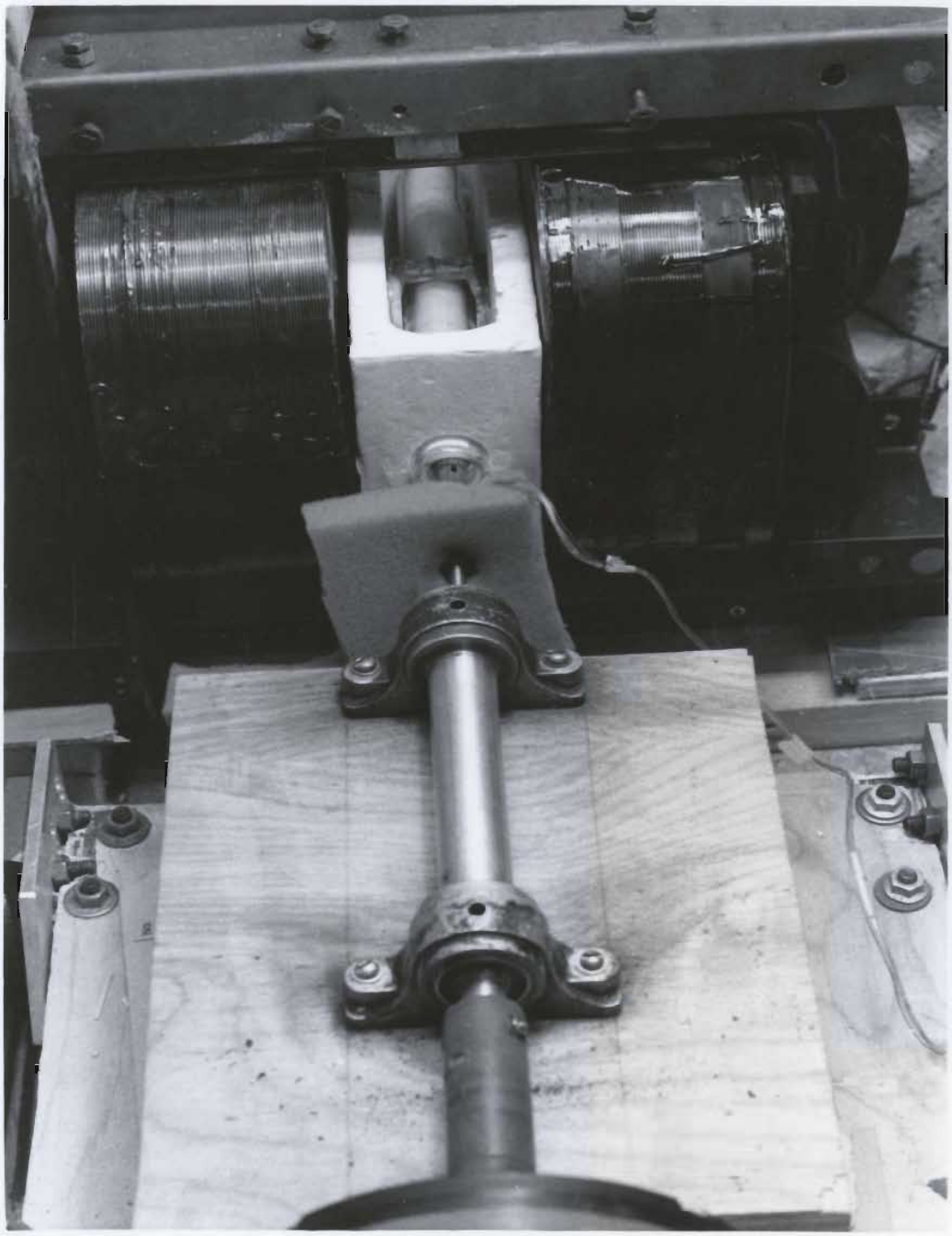

Figure 2.2: Photograph of vibrating-sample magnetometer.

in this thesis, making it easy to calibrate. I had to increase the magnet's original pole gap of 2.5 cm to 8.2 cm in order to accommodate the vibrating sample, the sample cooling system and the pick-up coils. The modified magnet produces a maximum field of approximately 3600 Oe (360 mT), when a current of 2.5 A at 145 V is passed through its coils. The field was found to be proportional to current (see section 2.7 for details).

Noise in the magnetic field delivered by the magnet must be avoided because it is detected by the pick-up coils reducing the magnetometer's sensitivity by decreasing the signal to noise ratio. It is thus essential that the power supply used for the magnet delivers a DC current free of noise and that this DC current be changed smoothly enough to avoid generating noise in the pick-up coils. The current was supplied by a DC power supply (Kepco Model JQE 150-7) which had very little AC ripple. The current was smoothly increased and decreased by a voltage supplied to the DC power supply by a triangle wave function generator (Hewlett Packard Model 3310A Function Generator) operating at a frequency of 0.005 Hz. This arrangement produced very little noise in the pick-up coils - orders of magnitude less than when the coils were placed in a commercial electromagnet with accompanying power supply (Varian Associates Model V3700-01 Magnet Assembly, and Model V2901 Regulated Magnet Power Supply).

2.3 The Sample Vibrator

A large sample is desirable since we are dealing with coarse-grained rocks. The sample must be vibrated at a constant frequency and amplitude. (An amplitude change of 10% for example will give an apparent change of 10% in magnetization.) The method of vibrating the sample consisted of rotating it on an off-axis shaft while preventing the sample from spinning. (Figure 2.3) To accomplish this, a main shaft was machined from aluminum with two stainless steel bearings placed within it with their centres 2 mm off the centre axis of the shaft. A second shaft was pressed into these bearings. A sample holder machined from a fibreglass epoxy resin material, Tufnol™, was then fixed to this second shaft using two set screws. By rotating the main shaft using a one third horsepower 120 V AC motor, the second shaft and its attached sample holder was moved around a circular path with 2 mm radius at 29.2 cycles per second. Meanwhile, the second shaft and sample holder were kept from rotating by a stationary foam rubber collar which kept the sample's orientation relative to the applied field constant.

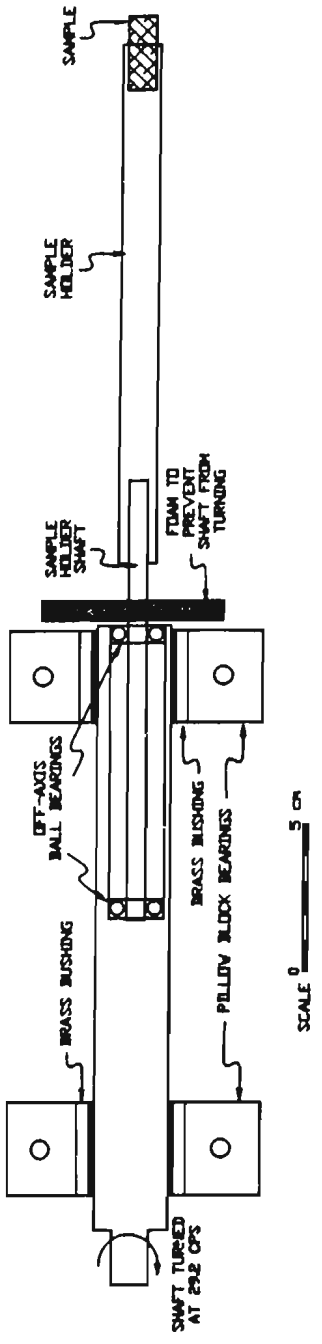

Figure 2.3: Drawing of the sample vibrator.

2.4 The Pick-up Coils

The placement of the sample with respect to the pick-up coils must be constant. With a single pick-up coil, a small variation in this placement could lead to serious changes in magnetometer sensitivity. It is very desirable to use a Helmholtz configuration of pick-up coils connected in series opposition to minimize this problem of placement. The series opposition configuration also helps reduce voltages induced in the pick-up coils due to variations in the applied field. The pick-up coils must also be isolated from the vibrating source so the coils do not vibrate relative to the applied magnetic field, inducing false voltages.

The pick-up coils, shown in Figure 2.4, were a matched pair of 3.8 cm diameter coils placed 3.1 cm apart (larger spacing than for a Helmholtz pair but still providing reasonably uniform pick-up sensitivity from the sample). Each coil was made of approximately 2000 turns of 34 AWG magnet wire and the two coils were connected in series opposition. The two coils were placed within the styrofoam liquid nitrogen container so that their axes were aligned and were perpendicular to the pole faces of the electromagnet. One coil was positioned squarely against each pole face with 0.64 cm of styrofoam intervening. Figure 2.5 is a photograph of the pick-up coils in place between the poles of the magnet.

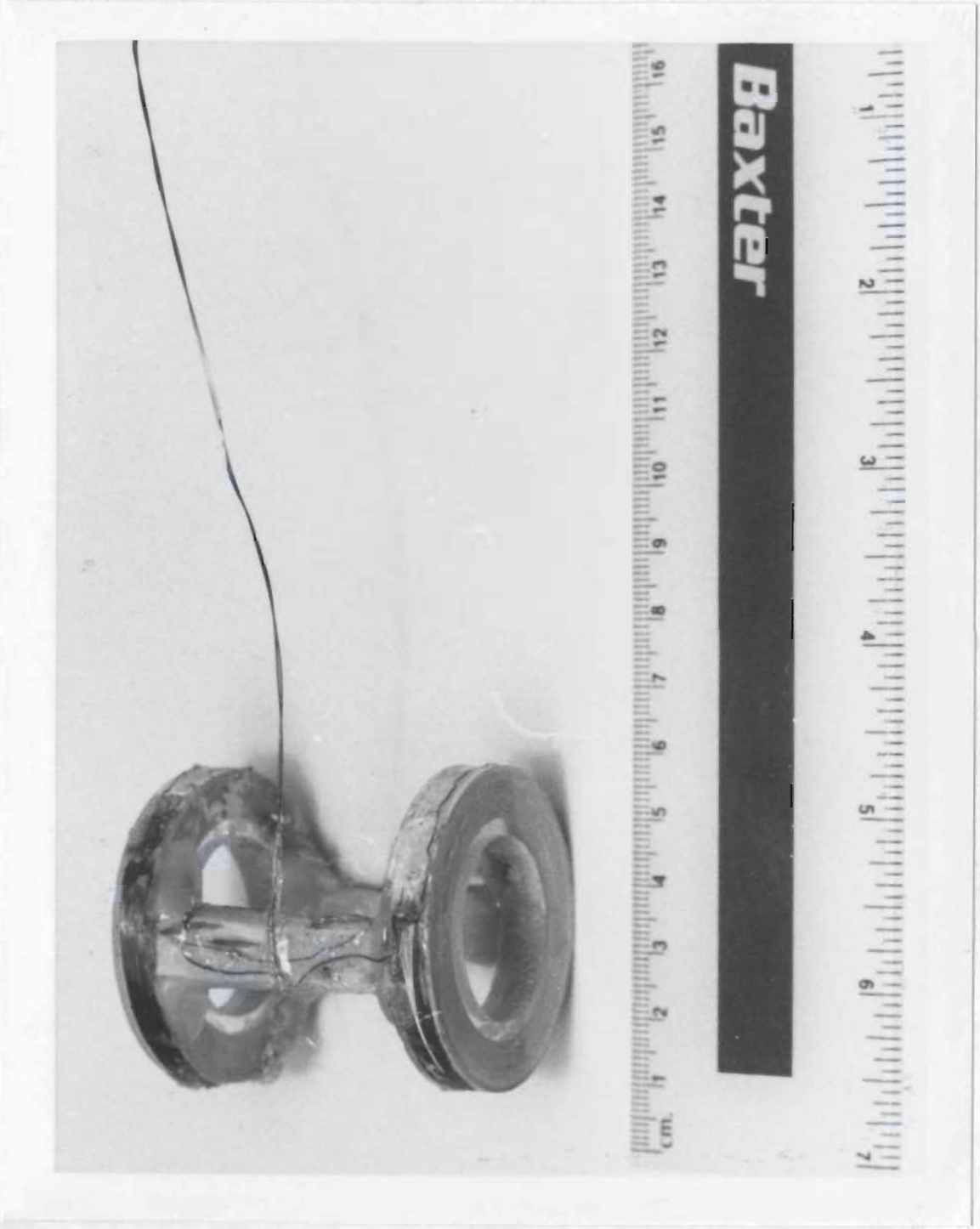

Figure 2.4: Photograph of the pick-up coils.

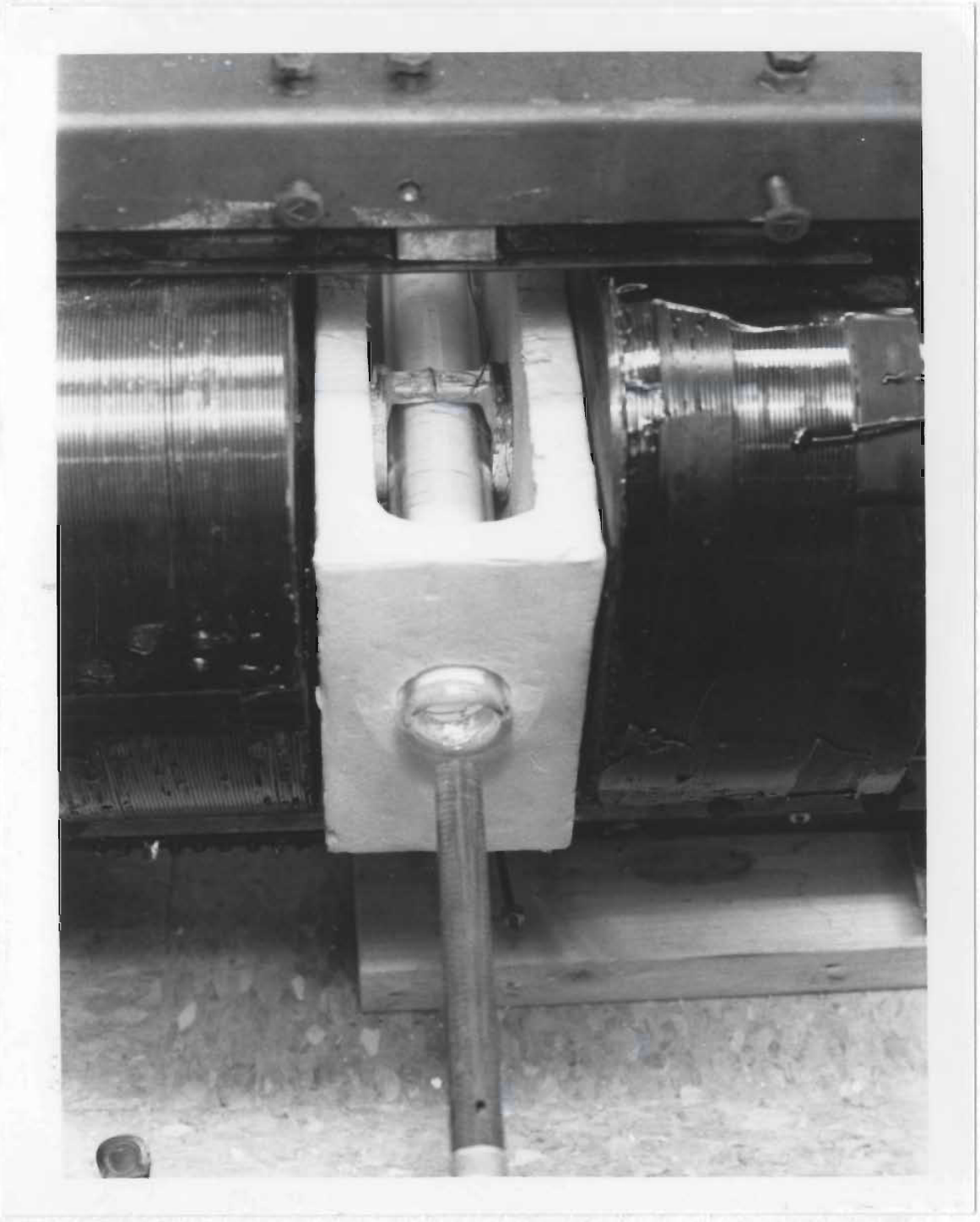

Figure 2.5: Photograph of the pick-up coils and the temperature control assembly installed in magnet.

2.5 The Temperature Control Assembly

The magnetometer design was also constrained by the need to vary sample temperature. To cool the sample, a liquid nitrogen container was constructed from styrofoam to fit snugly within the pole gap of the magnet. (Figures 2.5 and 2.6) This container also housed the pick-up coils and the sample port assembly. Figure 2.7 is a photograph of the temperature control assembly. Care was taken to use only non-magnetic materials in constructing all parts of the magnetometer (other than the magnet itself).

Within the pick-up coils is a sample port assembly which isolates the sample from the liquid nitrogen reservoir and contains a heating element. This assembly allows the sample to be vibrated at the centre of the coil pair and allows the temperature of the sample to be increased above that of liquid nitrogen. The sample port assembly consists of an open-ended Dewar flask 23 cm long with an inside diameter of 2.1 cm and an outside diameter of 3.1 cm. This Dewar was made by sealing the ends of two 2 mm thick Pyrex glass tubes, one with an outside diameter of 3.1 cm and the other with an outside diameter of 2.5 cm. The annular space between the two tubes was then evacuated with the aid of a small amount of charcoal getter and then sealed. The Dewar was then pushed through holes machined in both ends of the styrofoam liquid nitrogen container. The Dewar was designed with both ends open to room temperature air after it was found experimentally that a Dewar with a single open end produced a sizable

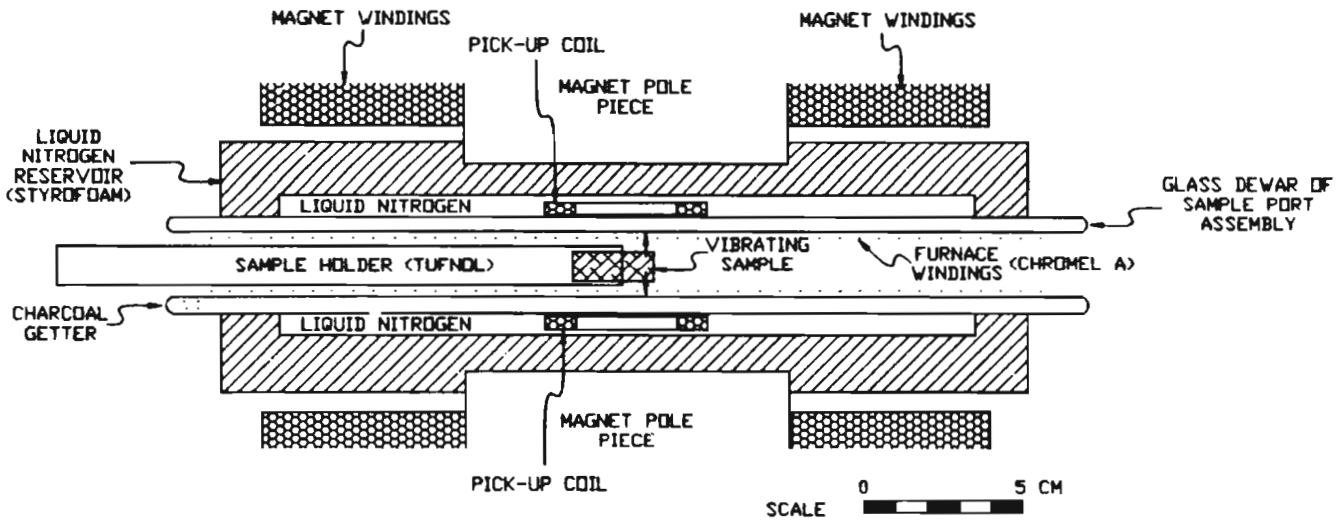

Figure 2.6: Drawing of the temperature control assembly.

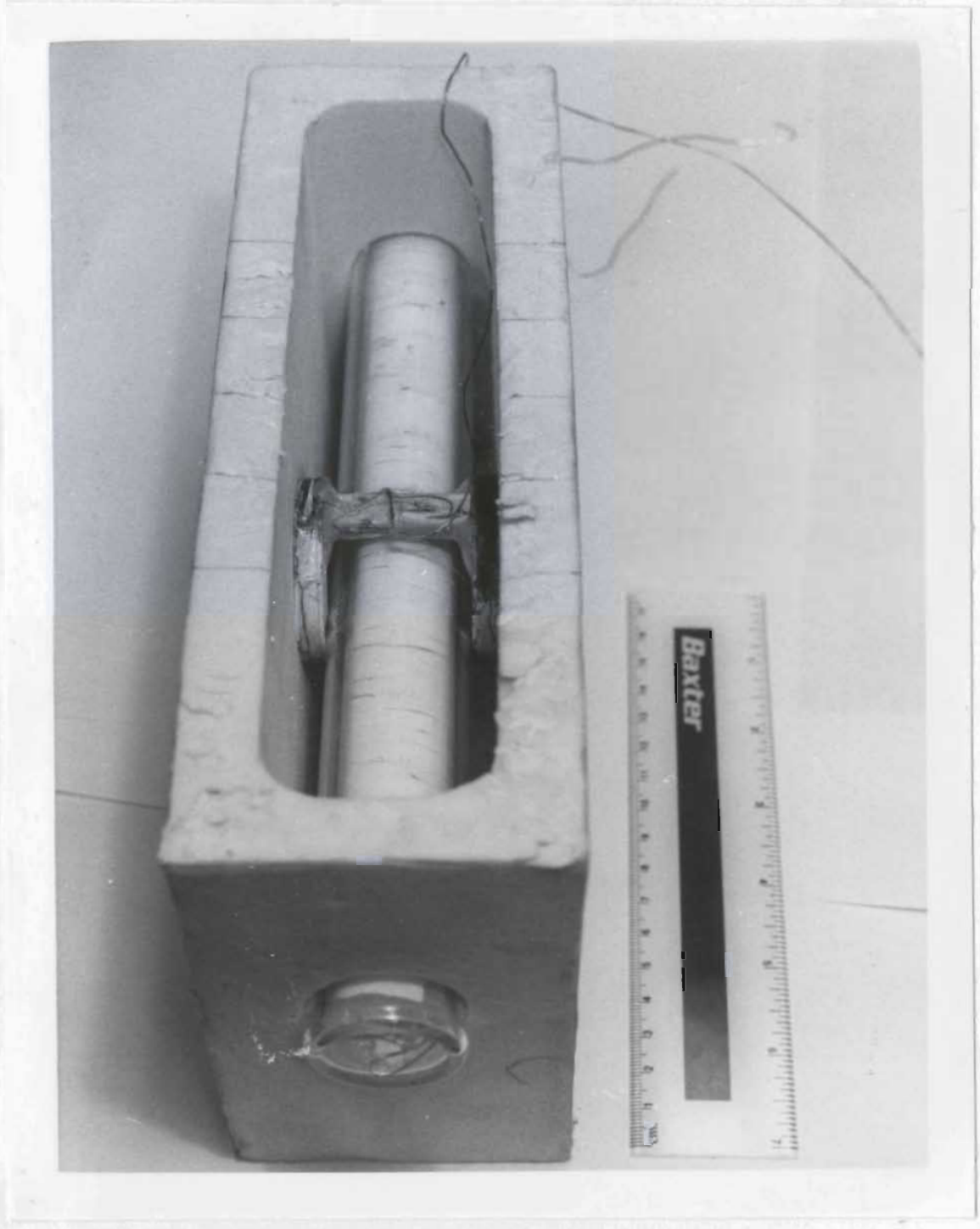

Figure 2.7: Photograph of the temperature control assembly and the pick-up coils.

temperature gradient along its entire length causing a few degrees of temperature difference between the ends of the vibrating sample.

The heating element fixed to the inside of the sample port assembly was constructed by winding a 4 metre length of Chromel A wire non-inductively. This element was attached to the inner wall of the Dewar with Ceramacast 520, a non-magnetic castable ceramic made by Aremco Products Inc. With liquid nitrogen surrounding the Dewar, the sample temperature within the sample port assembly could be varied from room temperature to near liquid nitrogen temperature by varying the current passed through the heating element from 1.75 to 0 A using a DC power supply (Kepco Model JQE 25-4). The sample's temperature could not be reduced to liquid nitrogen temperature (77 K), but only to about 98 K. This was mainly due to the insulating properties of the evacuated space in the Dewar and the fact that it was open to room temperature air at both ends.

Figure 2.8 is a graph of the cooling rates of various Dewars constructed during the study. It took many tries to achieve a cooling rate which would allow the temperature to approach liquid nitrogen temperature as well as allow the temperature to be stabilized near room temperature. The graph shows that a Dewar with too high a vacuum takes a very long time to reach the temperature of the liquid nitrogen. A Dewar with too little vacuum reaches liquid nitrogen temperature too quickly, and is very difficult to stabilize at temperatures close to room temperature. The vacuum in the Dewar was adjusted by varying the amount of charcoal getter used in the evacuated

space. The more charcoal used the higher the insulating properties of the Dewar. Once the cooling curve neared the desired level, the amount of vacuum was fine tuned by heating the charcoal thus reducing the vacuum.

The temperature inside the sample port was measured using two Copper-Constantin thermocouples (referred to as T type thermocouples). These were chosen because of their non-magnetic properties, their effective operating range from 423 to 73 K (+150 to -200°C), their high accuracy and their relatively low cost. One thermocouple was placed in the sample holder next to one end of the sample. The other thermocouple was inserted in through the opposite end of the sample port to a point near the other end of the sample. The two temperatures measured usually agreed to within a few degrees and their average was considered to be the temperature of the sample.

2.6 Measurement Procedure

First, we will discuss the equipment used to monitor magnet output, pick-up coil output and temperature. Then we will describe the procedure used to measure a sample's hysteresis loop. Pen and paper were used to record all pertinent data instead of using more costly digital data acquisition techniques.

Figure 2.9 shows the block diagram of the measuring system. The magnetic field applied to the sample was monitored by the horizontal axis of a Hewlett Packard Model 7000 AM X-Y recorder. A voltage that was proportional to the current passed through

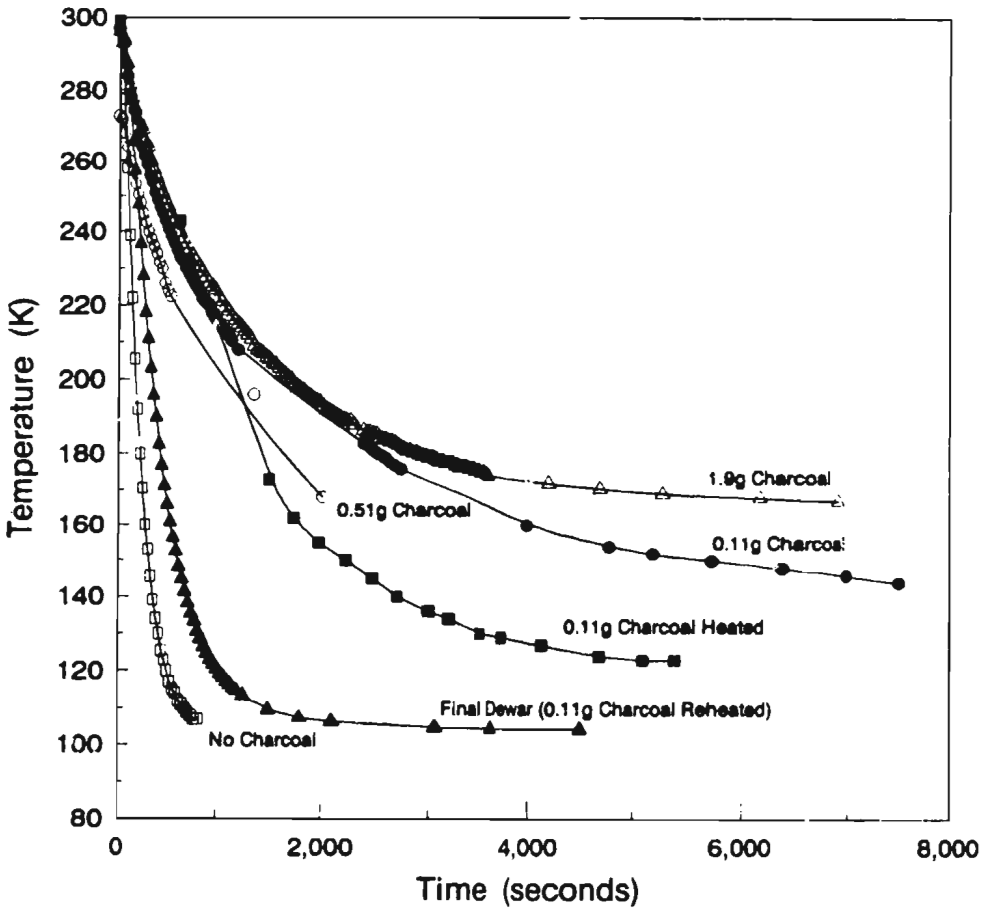

Figure 2.8: Plot of specimen temperature versus time for the various Dewar flasks tried in the temperature control assembly (from the time when the Dewar was first surrounded by liquid nitrogen). The Dewars differed in the amount of charcoal getter included to improve the vacuum and whether the getter was later heated to reduce the vacuum.

the coils of the magnet was applied to the horizontal (X) axis of the X-Y recorder. This voltage was measured across a 25 Watt 0.1 Ohm resistor placed in the circuit of the magnet coils.

The sample's magnetization was monitored by connecting the pick-up coils to a Tectronix Oscilloscope Model 561A allowing the output waveform to be monitored to be sure it was sinusoidal. In general, the output from the pick-up coils consisted of a main 29.2 Hz sinusoidal component with harmonics of this frequency superimposed. The harmonics are a function of the coil geometry, sample vibration amplitude and sample size relative to coil size. The signal from the pick-up coils was amplified and filtered by the oscilloscope using a Model 3A9 Differential Amplifier Module and applied to the vertical axis of the X-Y recorder.

A phase sensitive detector or lock-in amplifier could have been used to increase the signal to noise ratio as described by Foner (1959) but was not needed because of the high magnetite content of the samples studied. This technique can allow measurement of signals obscured by noise up to three orders of magnitude larger than the signal and should be considered for less magnetic samples. A lock-in amplifier acts as a narrow band amplifier tuned to the frequency of the signal, and is followed by a rectifier. The output from the lock-in amplifier is a DC voltage proportional to the amplitude of the fundamental frequency of the signal and the cosine of the difference in phase between the measured signal and a reference signal of the same frequency. A common method of generating a reference signal is with a pick-up coil close to a small magnet attached

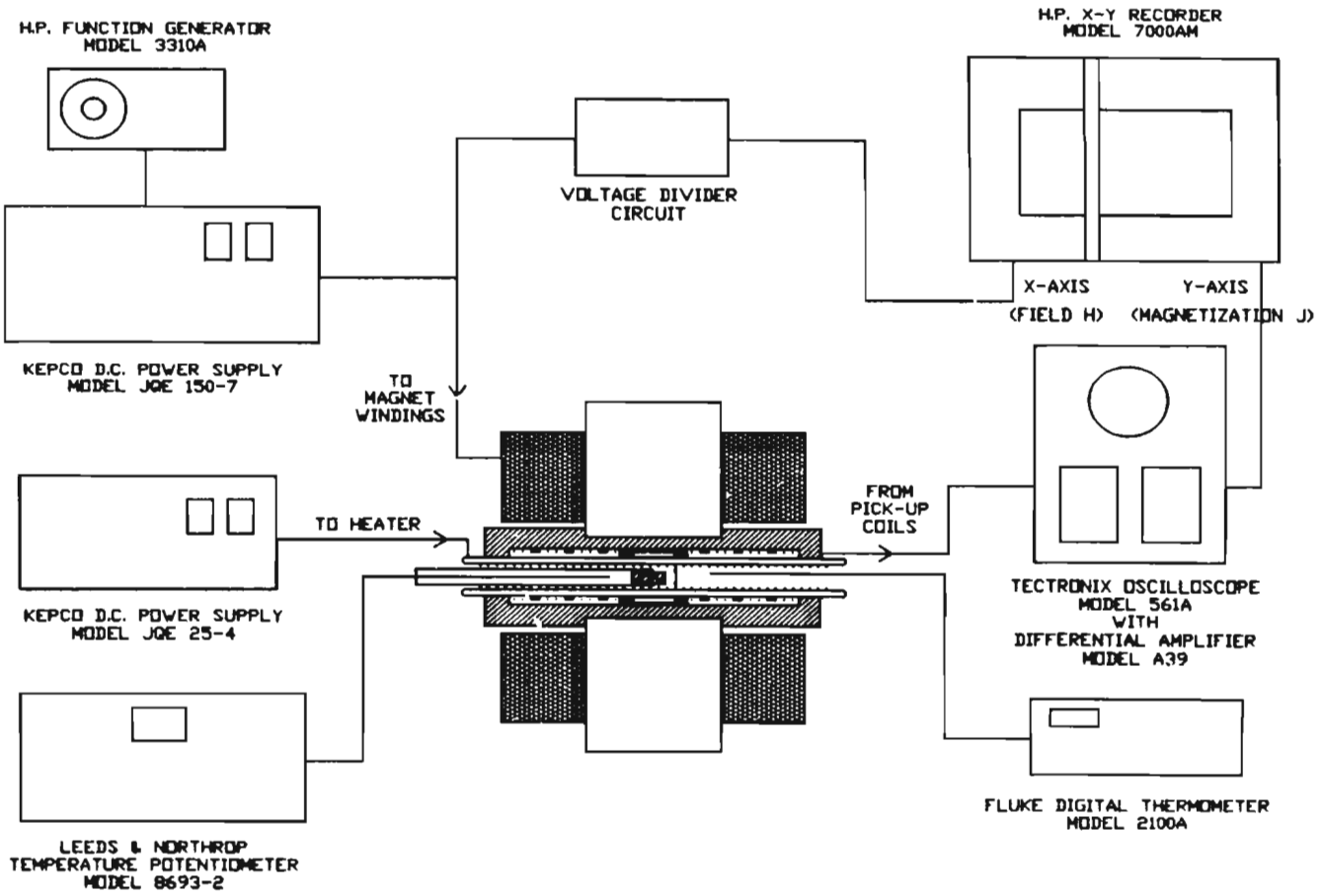

Figure 2.9: Block diagram of the measuring system.

to the vibrator shaft.

The horizontal axis of the X-Y recorder was used to plot the magnetic field (H) applied to the sample, while the vertical axis of the recorder was used to plot magnetization (J) of the rock sample. The field was cycled from 0 to 3600 Oe (360 mT) to 0 again and half the hysteresis loop was automatically traced. Then the polarity of the applied field was reversed and the second half of the hysteresis loop was traced. This procedure could be repeated for temperatures from near room temperature to 98 K (-175°C).

Figure 2.10 is an actual plot of half a hysteresis loop plotted on the X-Y recorder. Note that the noise level slightly increases as the field is increased, but noise still remains a small fraction of the signal level.

Temperature was monitored by connecting one of the Copper-Constantin thermocouples to a Leeds and Northrop Temperature Potentiometer Model 8693-2 and the other thermocouple to a Fluke Digital Thermometer Model 2100A. The Leeds and Northrop Temperature Potentiometer needed to be "zeroed" manually before the temperature could be read off its calibrated scale and recorded. The Fluke Digital Thermometer displayed the temperature "in real time" on its LED display allowing the temperature to be monitored constantly during the experiment.

2.7 Calibration of the Field Axis

The field axis (X) of the recorder was calibrated using a Bell Model 640 Gaussmeter with a probe used for measuring transverse magnetic fields.

First, the proportionality between the field produced by the magnet and the current passed through the magnet windings was checked. This was accomplished by connecting the output from the gaussmeter to the vertical axis of the X-Y recorder while a voltage proportional to the current through the magnet windings was applied to the horizontal axis. As the current was increased, the magnetic field measured by the gaussmeter increased. Both increased in proportion as shown by the straight diagonal line drawn on the X-Y recorder to the highest fields used, 3600 Oe (360 mT). The magnet's laminated iron core helped produce this proportionality as well as reducing remanence in the pole pieces. There was only a very small field of less than 5 Oe (0.5 mT) left in the pole gap after the magnet was cycled to maximum field and then back to zero.

To calibrate the field axis (X), the gaussmeter was disconnected from the X-Y recorder and a battery with a momentary on switch was connected in series to the Y axis. The current applied to the magnet was then slowly cycled, from zero to maximum and back to zero. While watching the field being measured by the gaussmeter as the current cycled, tick marks were made on the recorder paper by pressing the momentary switch when the gaussmeter displayed a multiple of 100 Oe. This was repeated for the

different scale settings on the recorder, using different multiples. In this manner a calibration factor (Oe/cm) was determined for each of the scale settings of the horizontal axis of the X-Y recorder.

2.8 Calibration of the Magnetization Axis

The first step in calibrating the magnetization axis (Y) of the recorder was to check that the vibration amplitude of the sample remained constant as the applied field was increased. Due to gradients in the applied field, the sample might be pulled sideways increasingly as field increased causing the vibration amplitude to increase with field. Such an effect would superimpose a spurious linear magnetization increase with field on the hysteresis loop of a ferromagnetic sample.

An experiment was designed to determine if there was any change in vibration amplitude with applied field. The sample was replaced by a small coil of wire of similar weight and size to a sample, and wound with its axis parallel to the applied field. A current of 0.5 A was passed through this coil to mimic a sample with a strong magnetization. The coil was thus vibrated, at room temperature, while the magnet field was cycled from 0 to 3600 Oe (360 mT). The signal in the pick-up coils did not change as the magnet field was cycled proving that the vibration amplitude of the sample does not change as applied field is cycled - at least not at room temperature.

To check if vibration amplitude changed as the temperature was decreased to

near liquid nitrogen temperature, a plot was made of percent change of saturation magnetization (relative to room temperature magnetization) versus decreasing temperature using sample SD78-0444. This plot, shown in Figure 2.11, shows the data from my vibrating-sample magnetometer, plotted as points, as well as the data of Pauthenet (1950) for magnetite plotted as a line. Except for the data collected at the two lowest temperatures, my data agree to within 1 percent with Pauthenet's data. Hence, the vibration amplitude can be considered constant, usually to within 1 percent.

The magnetization axis was then calibrated by assuming that saturation magnetization J_S = 480 emu/cm^3 for magnetite in the sample. None of my samples saturated in 3600 Oe (360 mT) but the method described by Bozorth (1951) was used to extrapolate to infinite field. Several points were picked from the hysteresis loops near saturation. These values of J in centimetres were plotted against 1/H in Oersteds using spread-sheet software (Lotus 123™). The least squares fit line was then extrapolated to 1/H = 0 (infinite field) to determine J_S in centimetres. Knowing that J_S = 480 emu/cm^3 allowed the J axis to be calibrated in terms of emu per cm^3 of magnetite in the sample.

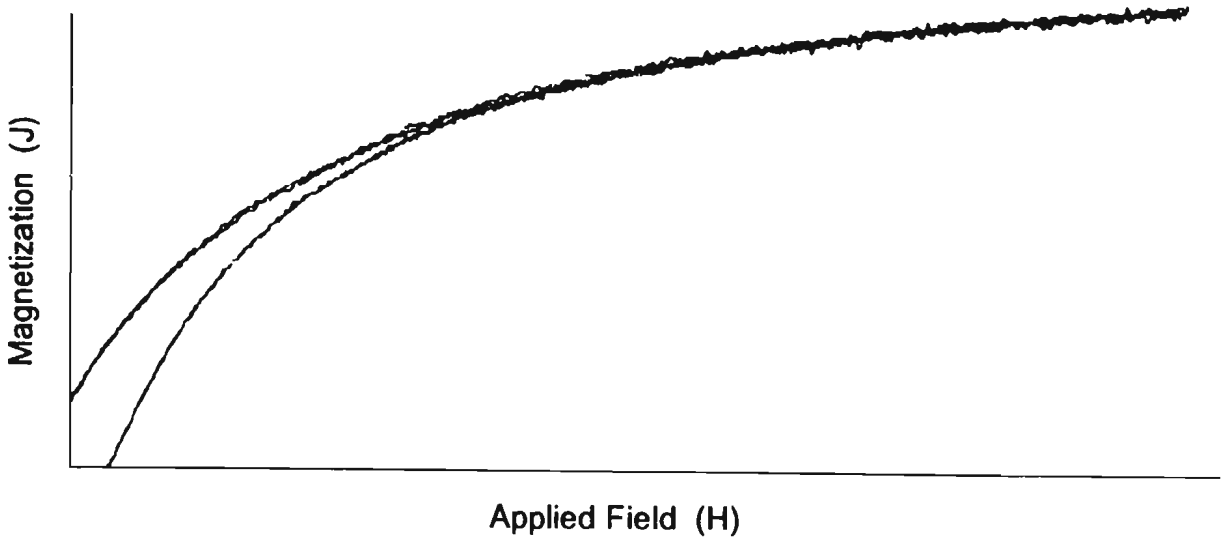

Figure 2.10: Hysteresis loop as recorded on XY plotter (reduced to 58% of original size).

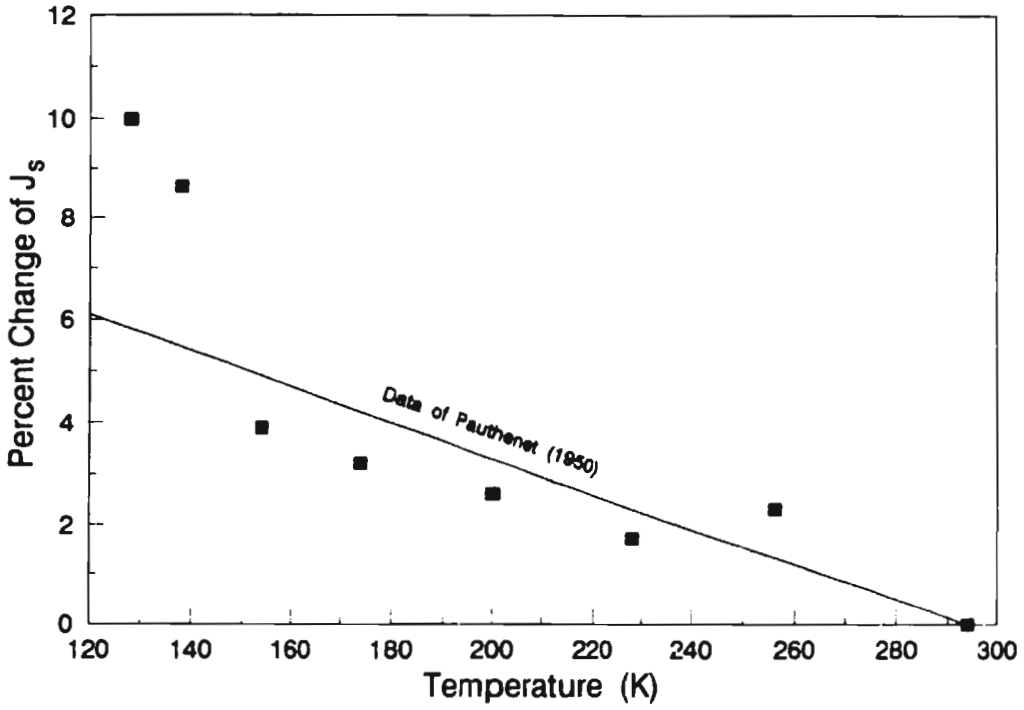

Figure 2.11: Percent change in saturation magnetization J_S versus temperature observed for sample SD78-0444 compared with the data of Pauthenet (1950).

CHAPTER 3

EXPERIMENTAL RESULTS

3.1 Selection of Samples

Seven Precambrian dolerite dyke samples were selected for use in the vibrating-sample magnetometer. The Matachewan and Biscotasing samples have been shown to carry primary remanence (Buchan and Halls, 1990). The Nain samples are from an east-west trending dyke swarm which likely carries a primary remanence (Buchan and Hodych, personal communication). They were chosen because they were magnetite-bearing, as suggested by their Verwey transition temperature (between 128 and 118 K), and because they displayed a range of high coercive force values. Table 3.1 is a listing of the sample numbers, the dyke swarm from which the samples were collected, the radiometric age of the dyke swarm and the coercive force of the samples measured at room temperature. The ages of the dyke swarms were determined by Uranium-Lead dating, except for the Biscotasing swarm which was dated using the Argon-Argon technique.

Table 3.1: Sample description.

Sample ID#	Dolerite Dyke Swarm	Radiometric Age of swarm	H_c ($\times 10^3/4\pi$ A/m)
SD78-0444	Matachewan, Ontario	2452 ± 3 Ma	147 Oe
BX86100502	Biscotasing, Ontario	2150 ± 3 Ma	125 Oe
25.7.91-16.1A	Nain, Labrador	1277 ± 2 Ma	103 Oe
25.7.91-28.2C	"	"	380 Oe
25.7.91-38.1A	"	"	210 Oe
EC91020101	"	"	326 Oe
EC91440101	"	"	487 Oe

3.2 Experimental Procedure

Hysteresis loops for the seven whole rock samples listed in Table 3.1 were plotted at temperatures ranging from room temperature (~294 K) to 98 K using the vibrating-sample magnetometer described in Chapter 2. Before any measurements could be made, the liquid nitrogen reservoir in the sample temperature control assembly had to be filled. The liquid nitrogen level in the reservoir was monitored throughout the experiment and more was added to keep the sample port assembly completely immersed at all times. Once the reservoir was filled, a DC current was applied to the heating element to bring the temperature in the sample port close to room temperature. The sample was then placed in the sample holder and carefully positioned in the sample port so as to be centred between the pick-up coils. Sample temperature was monitored with the two thermocouples until thermal equilibrium was attained.

When the temperature stabilized, the sample was cycled several times through the hysteresis loop before plotting began. Then, the sample magnetization was plotted continuously as a function of field as the applied field was increased to 3600 Oe (360 mT) and then decreased to zero. This was then repeated with the field in the opposite direction.

Temperature was then lowered by decreasing the current passing through the heating element. When thermal equilibrium was again reached, another hysteresis loop was plotted as before. This was repeated for successively lower temperatures.

Temperature was measured to an absolute accuracy of ±3°C, using the average value from the two thermocouples, one positioned in the sample holder behind the sample and the other positioned in front of the sample on a stationary holder.

3.3 Experimental Results

Figures 3.1 to 3.4 show hysteresis loops plotted for the Matachewan dolerite (SD78-0444) at various temperatures (indicated near the top of each plot). Note that the hysteresis loops are slightly smoothed because they were digitized and plotted using Autocad™ computer drafting software. Figures 3.5 to 3.7 are room temperature hysteresis loops for the other six samples.

Along with the complete hysteresis loop to 3600 Oe (360 mT) shown, a second loop was always recorded using more sensitive plotter scales to show only the portion

of the loop close to the origin to make it easier to measure H_C and J_R accurately. Values for H_C and J_R were measured from the latter loops and are plotted against decreasing temperature in Figures 3.8 and 3.9 respectively.

Although coercive force and saturation magnetization are independent of self-demagnetizing fields, saturation remanence is not. To correct for the shearing effect of self-demagnetizing fields, the self-demagnetizing factor N had to be estimated. For this study, N was considered to be equal to H_C/J_R although this may be an overestimate of N (Hodych, 1986a) and for small numbers of domains per grain (high coercive force) N can vary somewhat with magnetization (Dunlop, 1983). All the points on the observed hysteresis loops would have to be moved horizontally a distance of NJ to correct for self-demagnetizing fields as shown in Figure 3.10.

After the self-demagnetizing factor was calculated, an estimate (corrected for self-demagnetization) was made of the reversible work done on the descending branch of the hysteresis loop. This was done with the aid of Autocad™ computer drafting software. First, a horizontal line was drawn at a constant magnetization near that produced at room temperature by the 3600 Oe (360 mT) field. Then the area was measured between this horizontal line, a line of slope 1/N drawn through the origin and the top of the hysteresis loop. This area is shown dotted in Figure 3.1 to 3.7. This area was then converted to the appropriate units using the conversion factors calculated in Sections 2.7 and 2.8, and plotted against decreasing temperature. Figure 3.11 is a plot of the reversible work versus temperature data. Note that the data for EC91440101 is

shown as a dashed line as it was not reliable below approximately 173 K because of noise of unknown origin so it was not included.

The above reversible work (W_{rev}) is integrated to constant magnetization. The reversible work integrated to constant field was calculated in a similar manner (the horizontal line corresponds to the magnetization produced by 3600 Oe rather than the constant magnetization as temperature is lowered) and is displayed as a function of temperature in Figure 3.12. Again the data for EC91440101 is shown as a dashed line because it was not reliable because of noise of unknown origin.

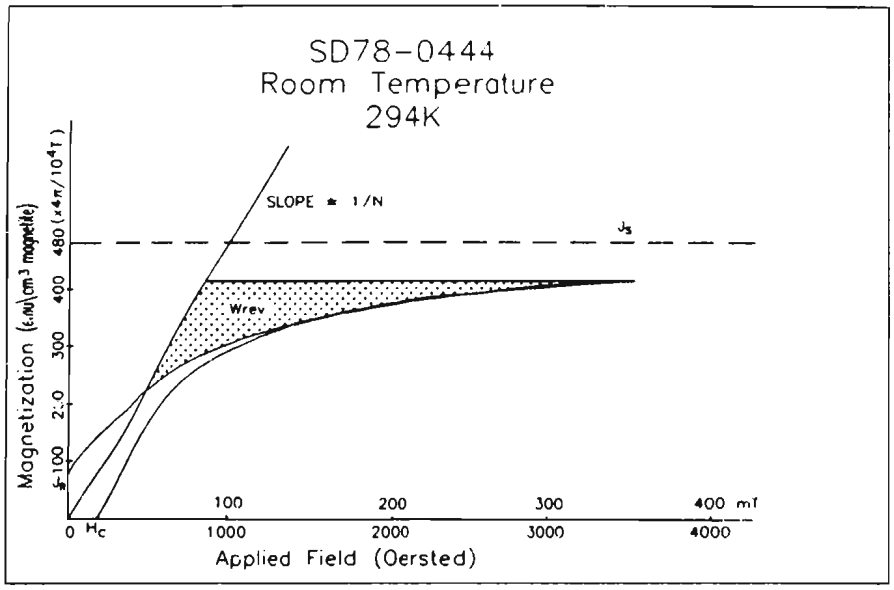

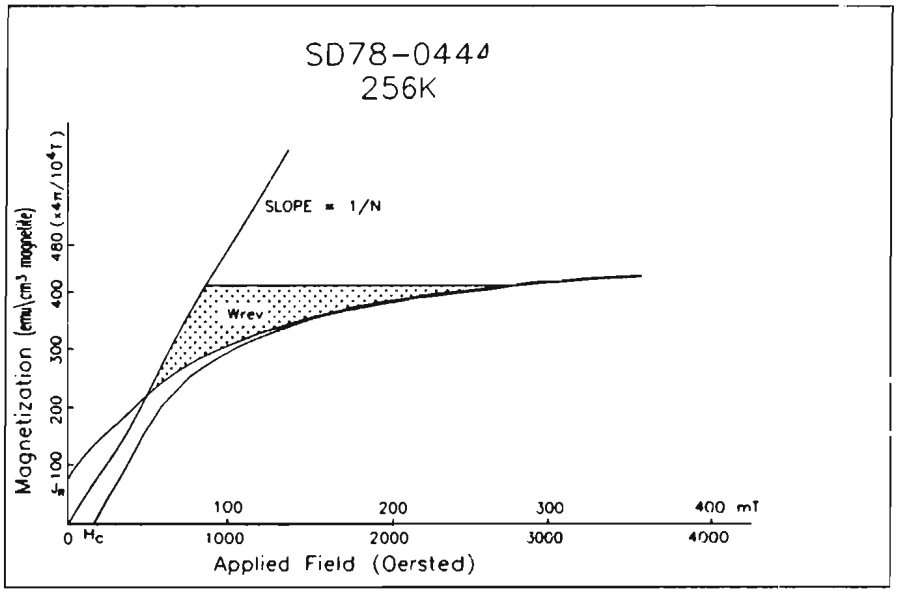

Figure 3.1: Hysteresis loops for Matachewan dolerite dyke sample (294 and 256 K).

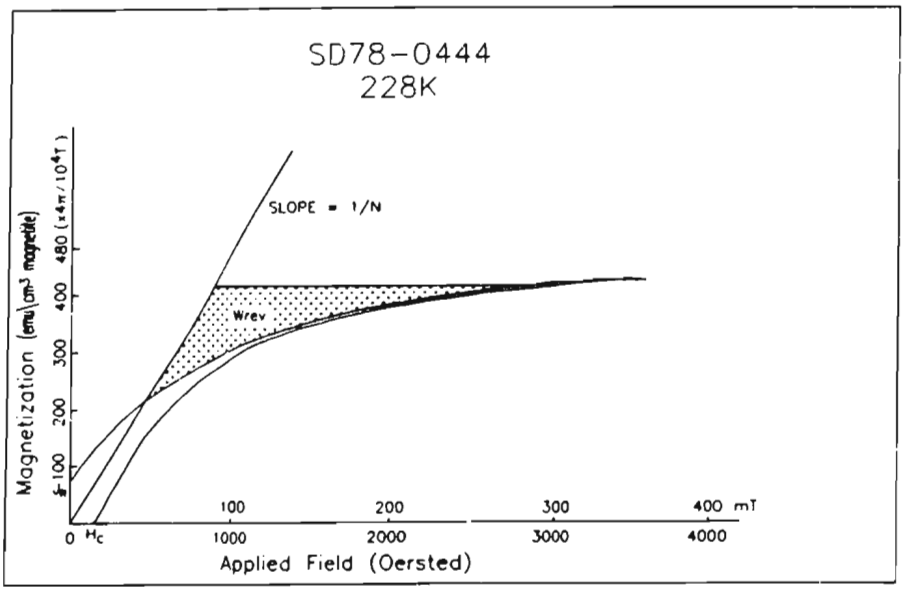

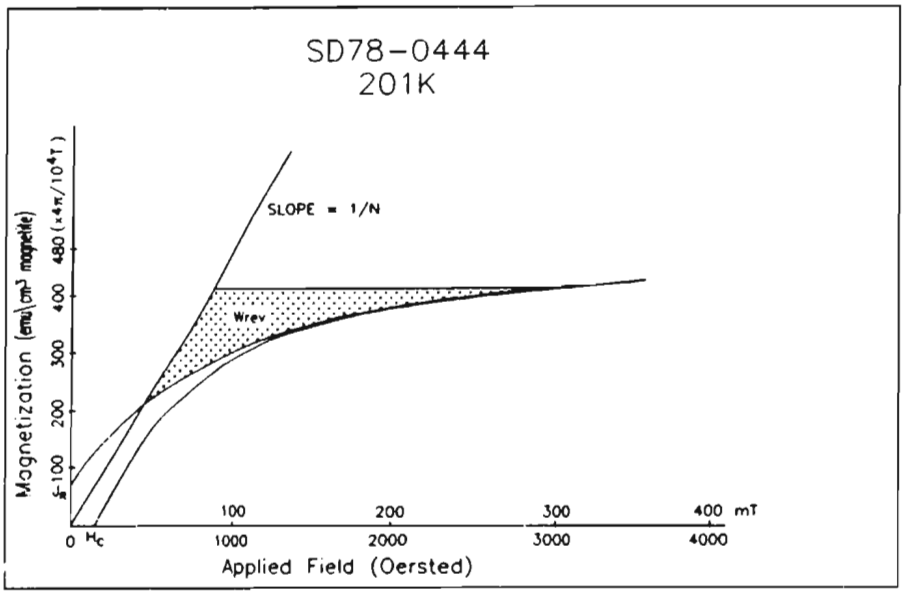

Figure 3.2: Hysteresis loops for Matachewan dolerite dyke sample (228 and 201 K).

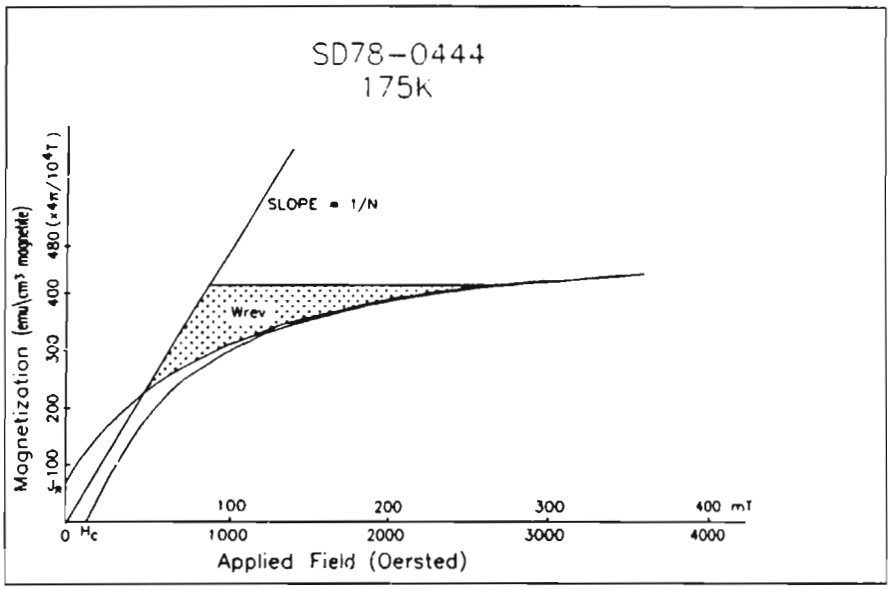

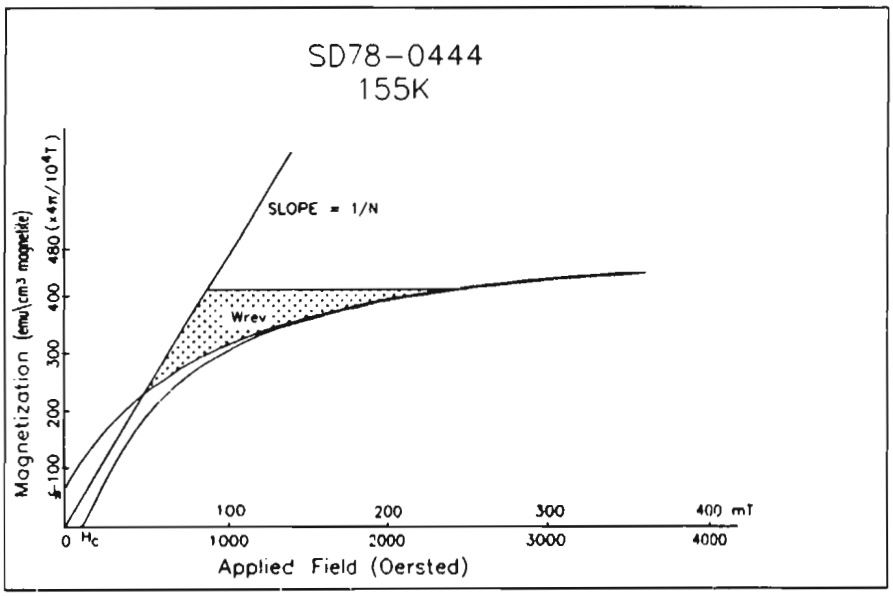

Figure 3.3: Hysteresis loops for Matachewan dolerite dyke sample (175 and 155 K).

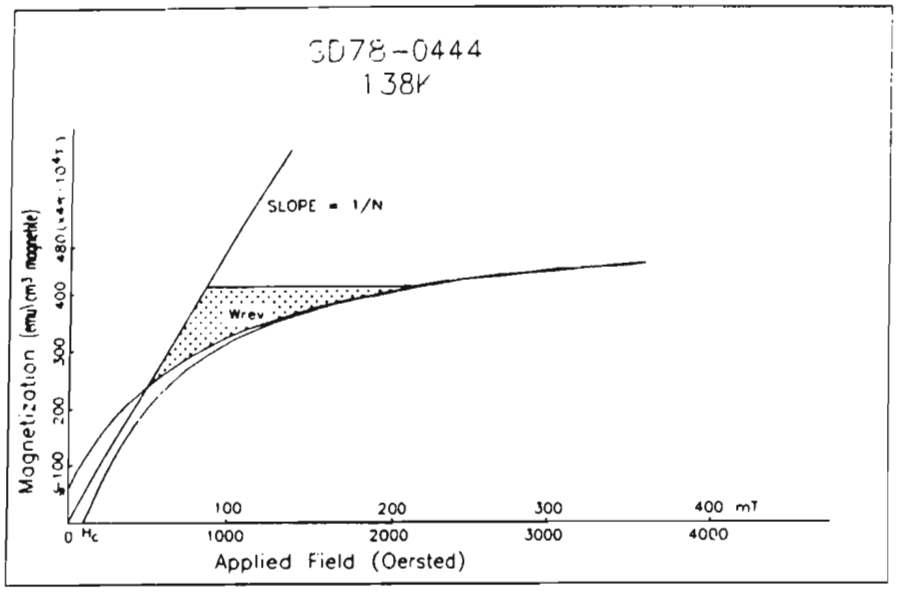

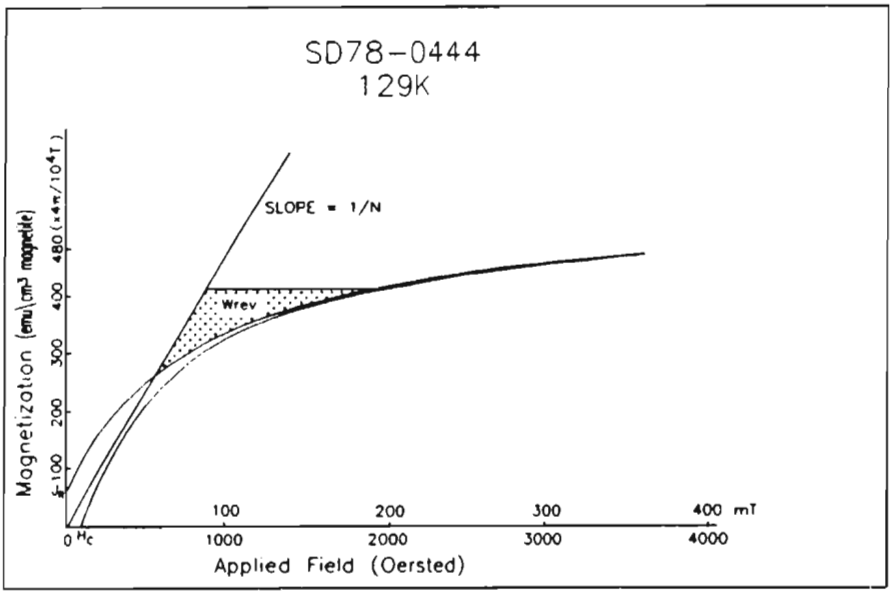

Figure 3.4: Hysteresis loops for Matachewan dolerite dyke sample (138 and 129 K).

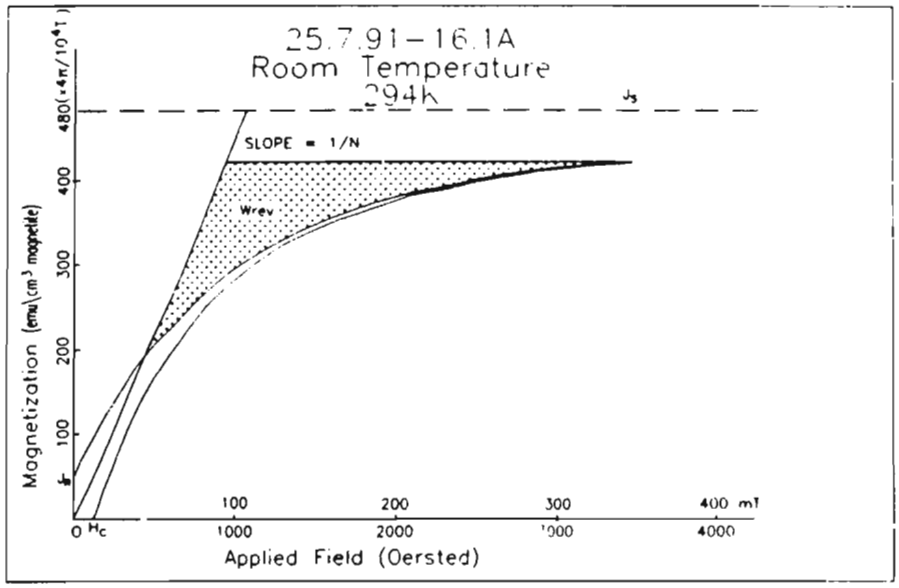

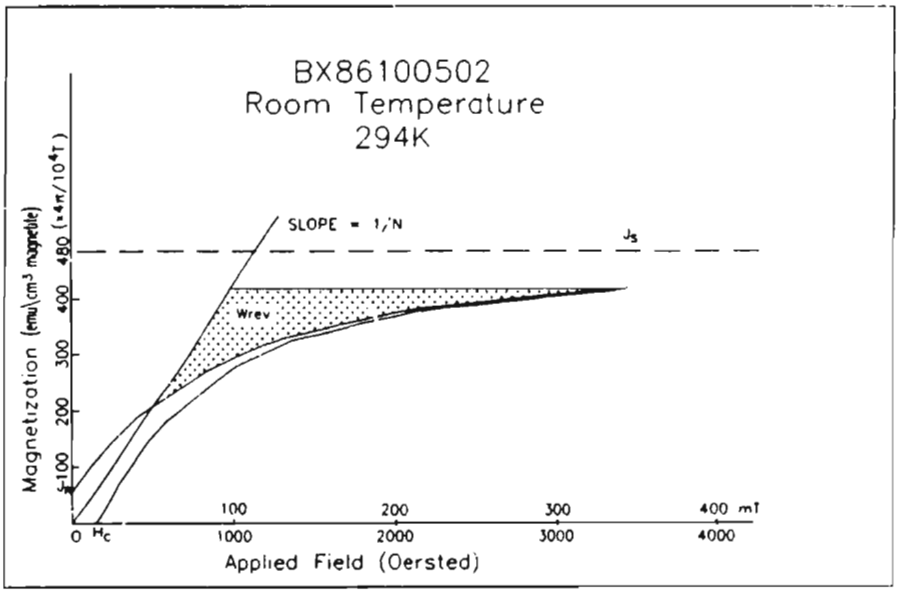

Figure 3.5: Room temperature hysteresis loops for Nain (above) and Biscotasing (below) dolerite dyke samples.

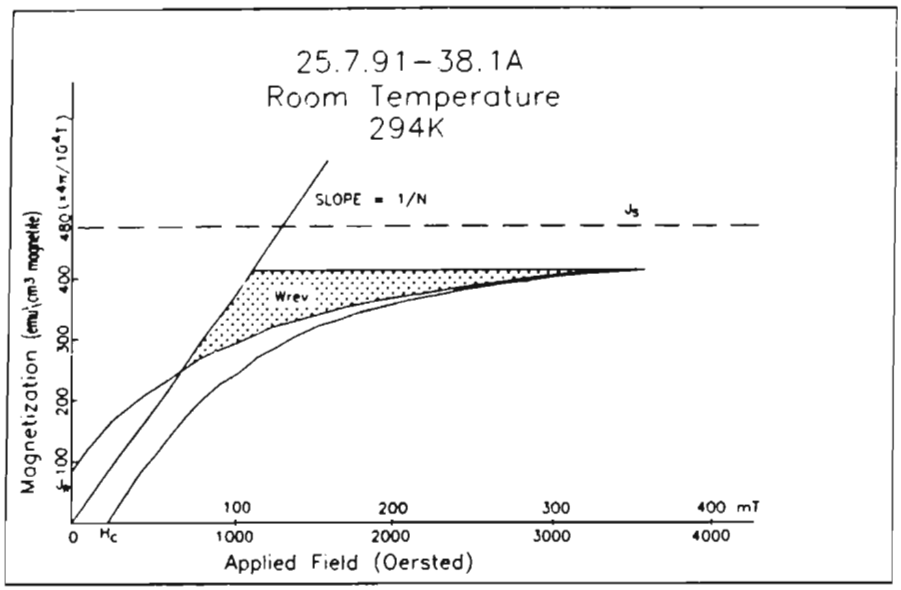

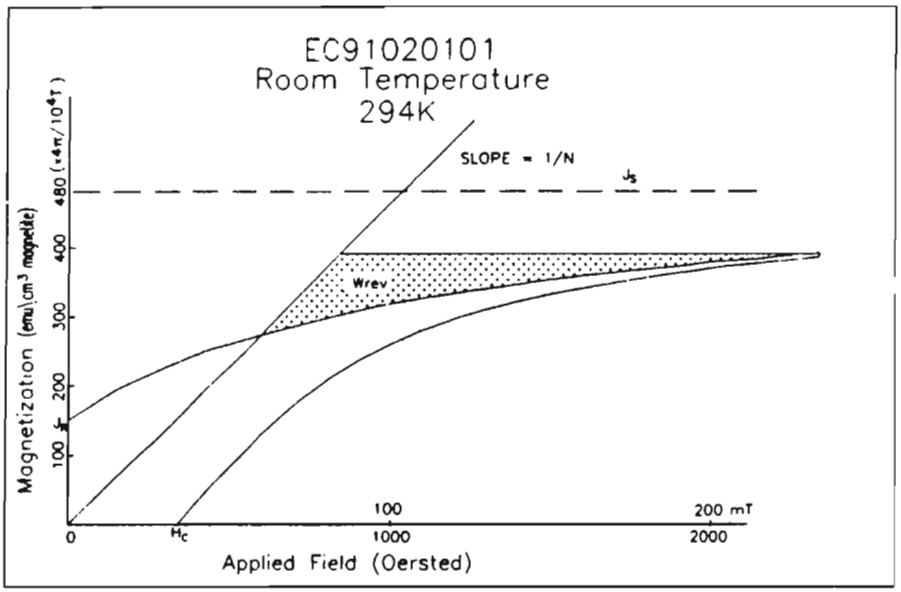

Figure 3.6: Room temperature hysteresis loops for Nain dolerite dyke samples.

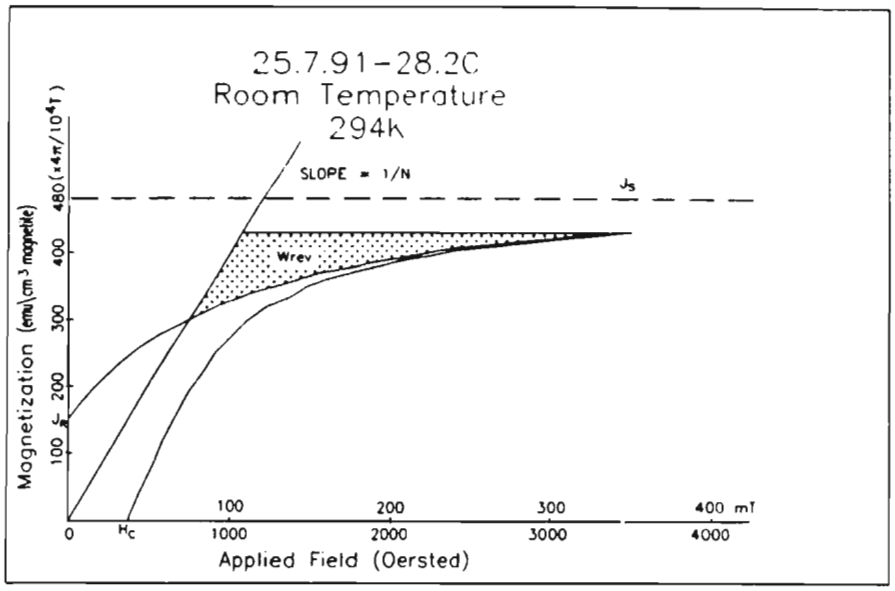

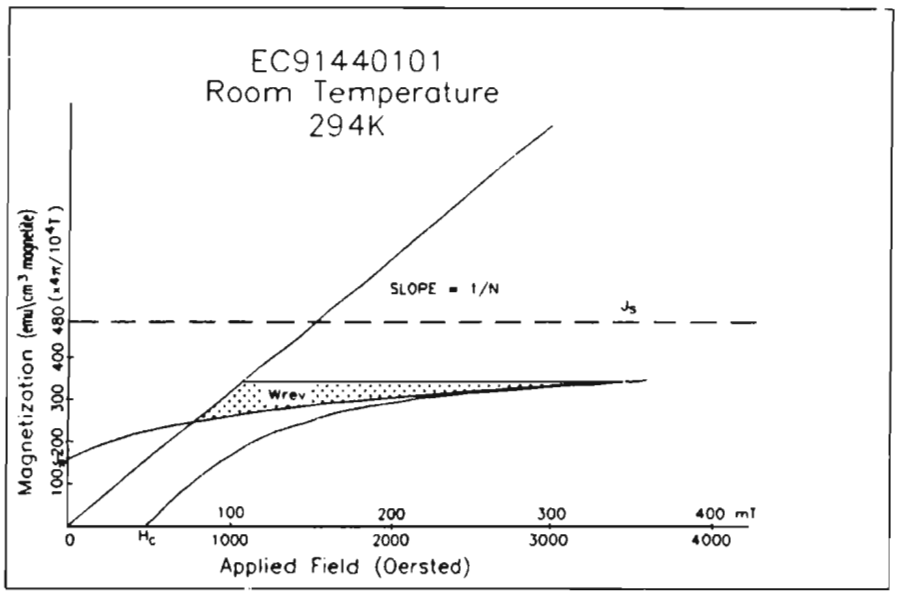

Figure 3.7: Room temperature hysteresis loops for Nain dolerite dyke samples.

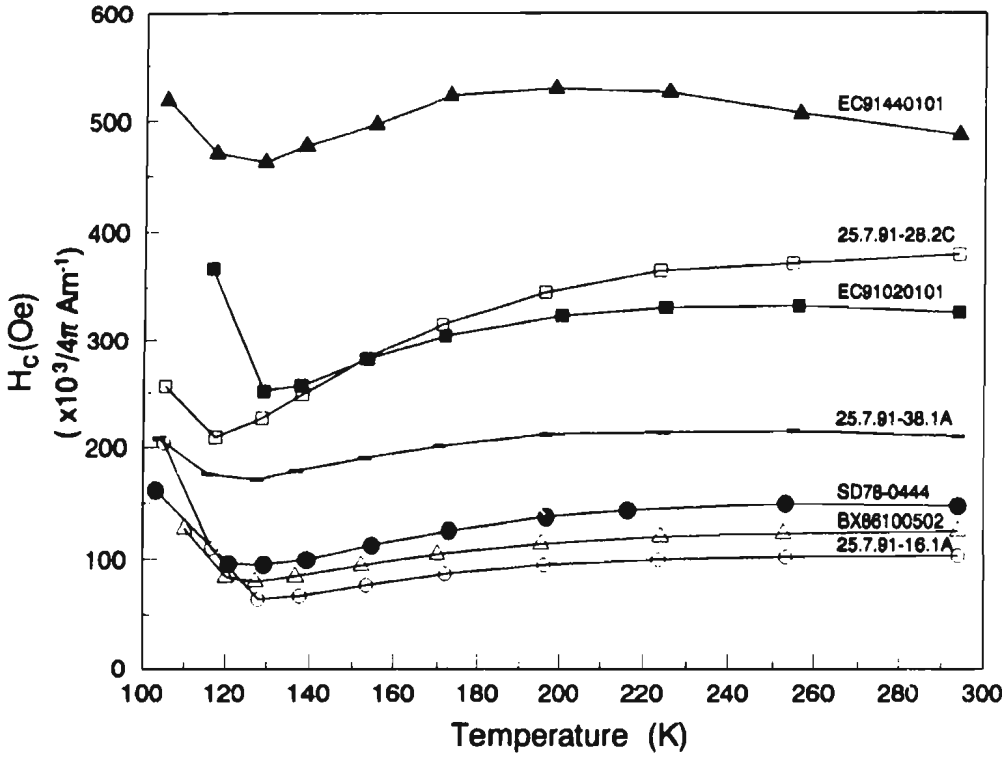

Figure 3.8: Coercive force H_c versus temperature observations.

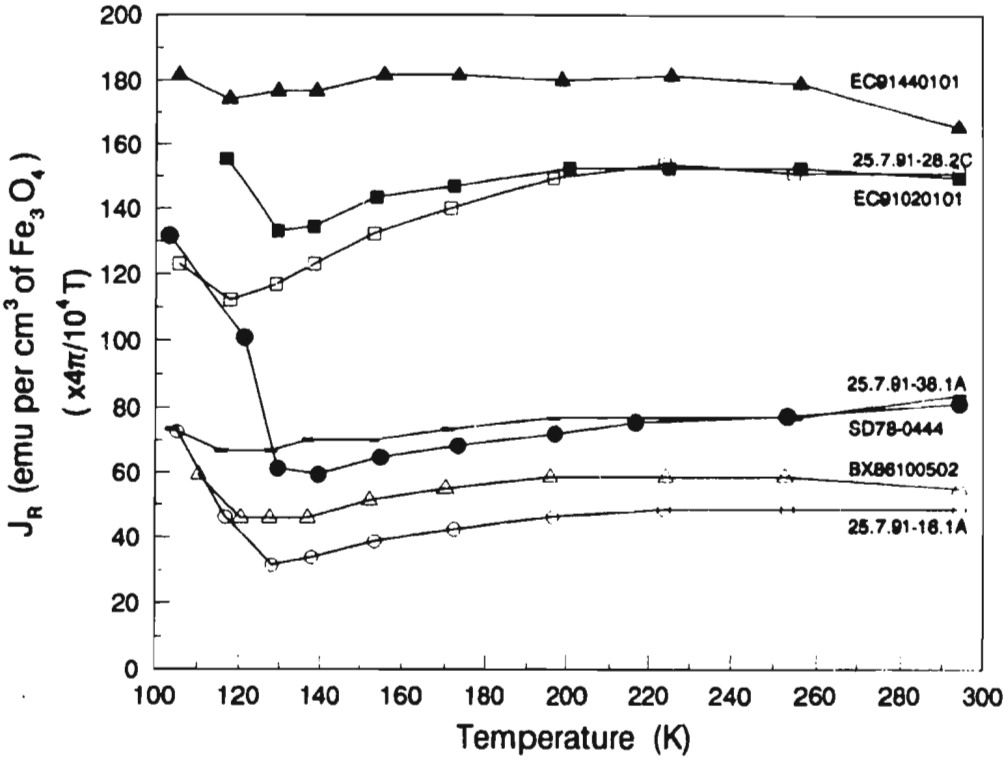

Figure 3.9: Saturation remanence J_R versus temperature observations.

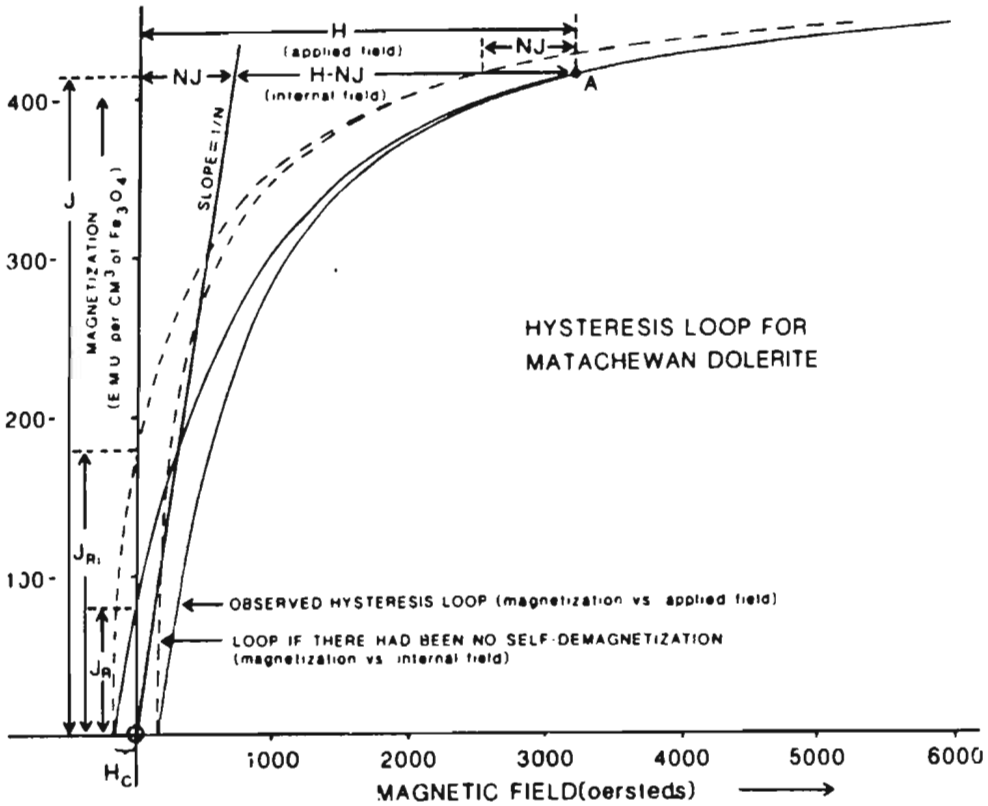

Figure 3.10: Effect of self-demagnetizing factor N on hysteresis loop for sample SD78-0444, from (Hodych, 1986a).

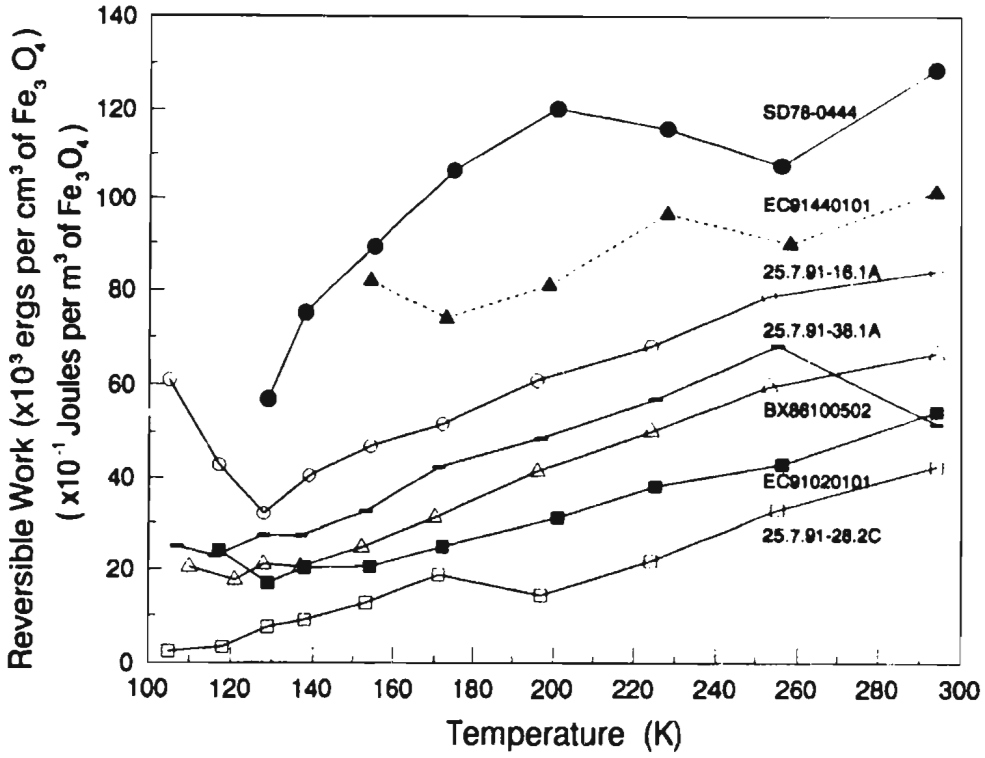

Figure 3.11: Reversible work W_{rev} (measured by integrating to constant magnetization) versus temperature observations.

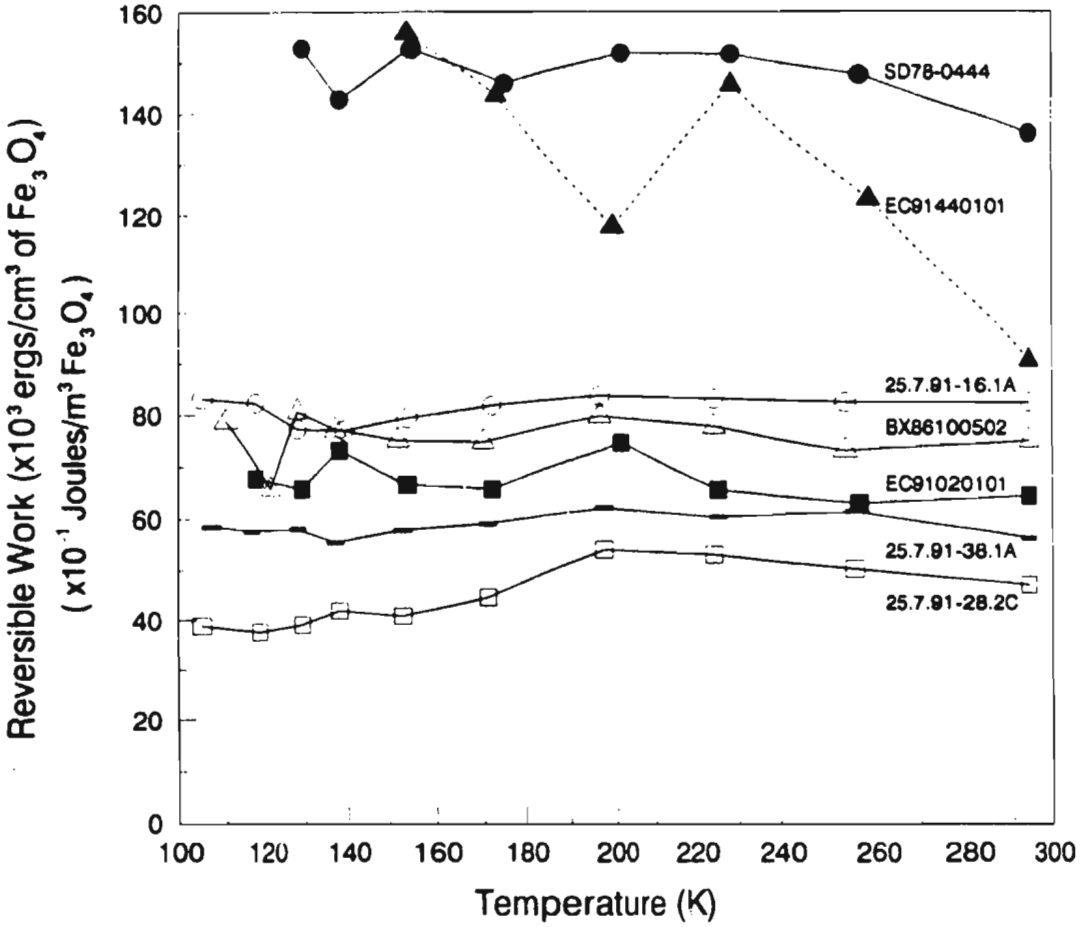

Figure 3.12: Reversible work W_{rev} (measured by integrating to constant field) versus temperature observations.

CHAPTER 4

INTERPRETATION OF RESULTS

4.1 Room Temperature Hysteresis Parameters

The seven rock samples selected for hysteresis measurement are all from dolerite dykes and hence they likely crystallized with relatively large titanomagnetite grains which on cooling exsolved into magnetite cut into fine grains by ilmenite lamellae. The fine intergrowth of magnetite and ilmenite makes grain size estimates difficult, as well as having the effect of lowering the self-demagnetizing factor (Davis and Evans, 1976).

Néel (1955) pointed out that, for rocks dominated by multidomain grains of magnetite of average self-demagnetizing factor N, one expects J_R/J_S to increase in approximate proportion to H_C since $N \approx H_C/J_R$. As seen in Figure 4.1, observed J_R/J_S for my dolerite samples does increase in approximate proportion to H_C (except perhaps for the highest coercive force sample). The inverse of the slope of the least-squares correlation line multiplied by the inverse of J_S is approximately 2.7 emu (2.2×10^6 H/m) which should give an estimate of the average self-demagnetizing coefficient, N. This value is significantly less than the $4\pi/3$ emu (3.3×10^6 H/m) expected of spherical grains presumably because of the non-magnetic ilmenite lamellae cutting the magnetite. Davis and Evans (1976) suggested that for simple magnetite-ilmenite lamellae in a cubic grain, the grain should have $N \approx f4\pi/3$, ($\div\mu_o$ in SI), where f is the volume fraction of ilmenite

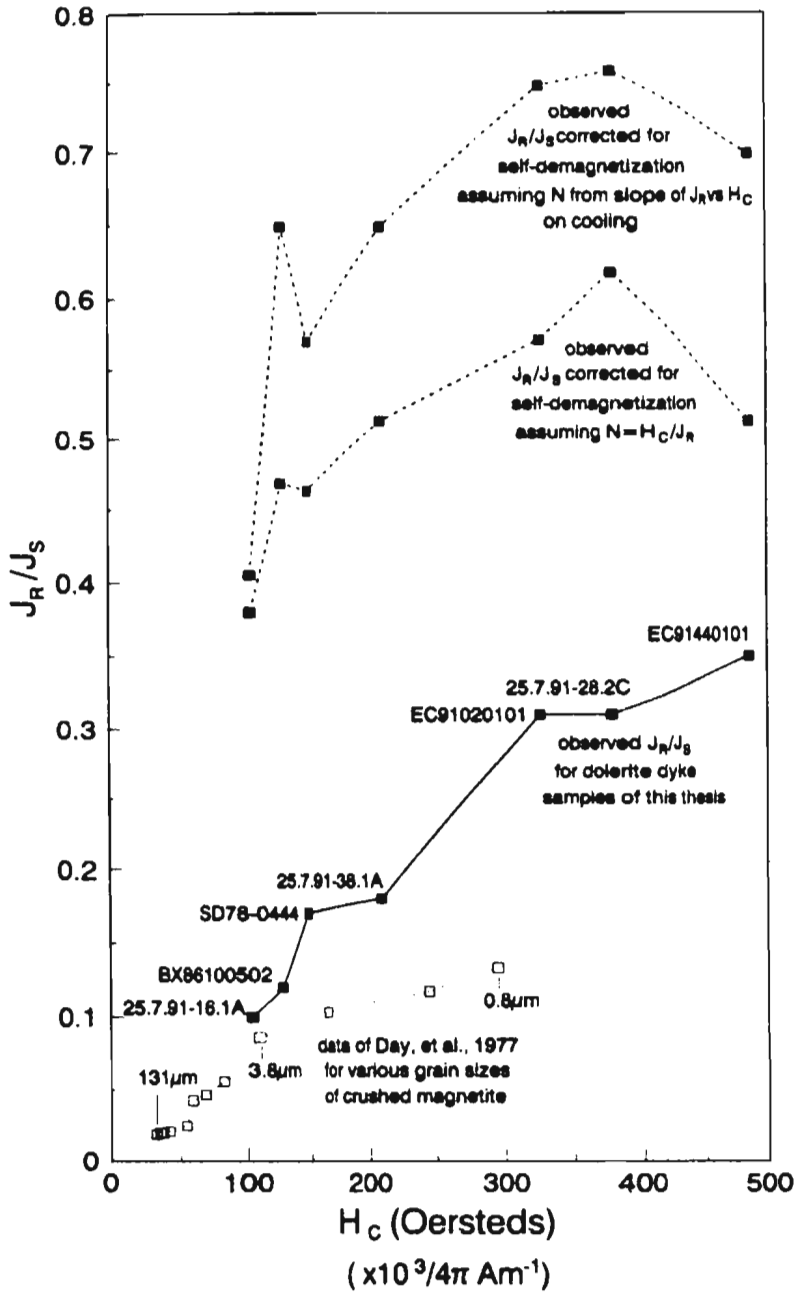

Figure 4.1: Ratio of saturation remanence to saturation magnetization J_R/J_S versus coercive force H_C observed for various samples at room temperature.

lamellae which should be approximately 0.4. A fraction 0.65 of ilmenite lamellae cutting the magnetite would account for my observed value of N inferred from J_R/J_S versus H_C. Also plotted in Figure 4.1 is J_R/J_S versus H_C, where J_R has been corrected for self-demagnetization assuming $N = H_C/J_R$. These corrected values of J_R/J_S are near 0.5 suggesting the presence of single-domain or pseudo-single-domain grains.

For comparison, Figure 4.1 also shows the data of Day et al. (1977) for pure magnetite ground under acetone in an agate mortar. One expects approximately equidimensional grains and therefore a self-demagnetizing factor of approximately $4\pi/3$ emu (3.3×10^6 H/m). The J_R/J_S values increase in approximate proportion to H_C with a slope suggesting $N \approx 4.6$ (3.7×10^6 H/m), agreeing reasonably well with the theory of Néel (1955). Some idea of the probable grain size of the magnetite in my dolerite samples can be obtained by comparing their coercive force values with those of the samples of Day et al. (1977). My lowest coercive force sample, 25.7.91-16.1A, could have an effective magnetite grain size of approximately 3.8 μm, and my three highest coercive force samples could have effective magnetite grain sizes of less than 0.8 μm.

4.2 Interpretation of H_C versus Low Temperature Results

The natural remanent magnetization (NRM) of terrestrial igneous rocks is often due to multidomain (or pseudo-single-domain) grains of magnetite (rather than single-domain grains). However, it is not clear what opposes domain wall motion in such

grains controlling coercive force (H_C) which is a measure of the stability of their remanence. Common theories (reviewed by Hodych 1982b), for control of coercive force in multidomain grains either have domain wall motion impeded by internal stresses leading to magnetostriction controlling H_C ($H_C \propto \overline{\lambda}_S J_o/J_S$) or they have domain wall motion impeded by inclusions leading to magnetocrystalline anisotropy controlling H_C ($H_C \propto |K_1| J_o/J_S$). For elongated single-domain grains, H_C should be controlled by shape anisotropy ($H_C \propto J_S$). The variation of saturation magnetostriction, $\overline{\lambda}_S$, and the magnetocrystalline anisotropy coefficient, K_1, with low temperature has been measured for magnetite by Bickford et al. (1955), and Syono (1965). By measuring hysteresis as a function of low temperature, one can infer what controls H_C by observing whether H_C varies in proportion to $\overline{\lambda}_S$ or $|K_1|$ on cooling or whether H_C shows little variation as expected of shape anisotropy control.

Figure 3.8 plots coercive force, H_C, as a function of decreasing temperature for each of the seven rock samples. The values of H_C decrease as the temperature is lowered from room temperature until between 128 and 118 K when a sharp increase in H_C takes place. This sharp increase is due to the Verwey transition at which magnetite changes its crystal structure from cubic to orthorhombic resulting in a large increase in magnetocrystalline anisotropy.

The coercive force measured at 140 K, H_C(140K), as a ratio of room temperature coercive force, H_C(294K), is plotted versus room temperature coercive force in Figure 4.2 for each sample. Lines representing the values of H_C(140K)/H_C(294K) expected for

coercive force controlled by shape anisotropy, stress-induced anisotropy and magnetocrystalline anisotropy are also shown. This plot should give a crude idea of which of the three anisotropies dominates the coercive force in the sample. The data displayed on the plot suggest that H_C for the sample with the highest coercive force, EC91440101, is dominated by shape anisotropy. Indeed this sample may be dominated by single-domain grains with shape anisotropy, in view of the very large coercive force (487 Oe, 3.9×10^4 A/m) and high J_R/J_S (0.35). The sample of next highest coercive force plots on the line for H_C dominated by stress-induced anisotropy, suggesting that high coercive force can also be due to internal stresses. The next two lower coercive force samples seem to have contributions to coercive force from both shape anisotropy and stress-induced anisotropy. Finally the three lowest coercive force samples seem to be mainly dominated by stress-induced anisotropy.

In Figure 4.3, the values of H_C observed on cooling were plotted against the corresponding values of $\overline{\lambda}_S J_o/J_S$, where $\overline{\lambda}_S$ is the polycrystalline saturation magnetostriction, calculated from $\overline{\lambda}_S = 0.4\lambda_{100} + 0.6\lambda_{111}$ using smoothed curves through the magnetostriction versus low temperature observations of Bickford et al. (1955). J_o is saturation magnetization at absolute zero and has a value of 520 emu/cm^3 (0.65 T). The variation of J_S on cooling is from observations of Pauthenet (1950). Coercive force was found to vary as a linear function of $\overline{\lambda}_S J_o/J_S$ as expected from the theory of Néel (1946) if H_C is mainly controlled by $\overline{\lambda}_S$ through internal stresses. The one exception is the sample of highest coercive force whose H_C is almost invariant with temperature as

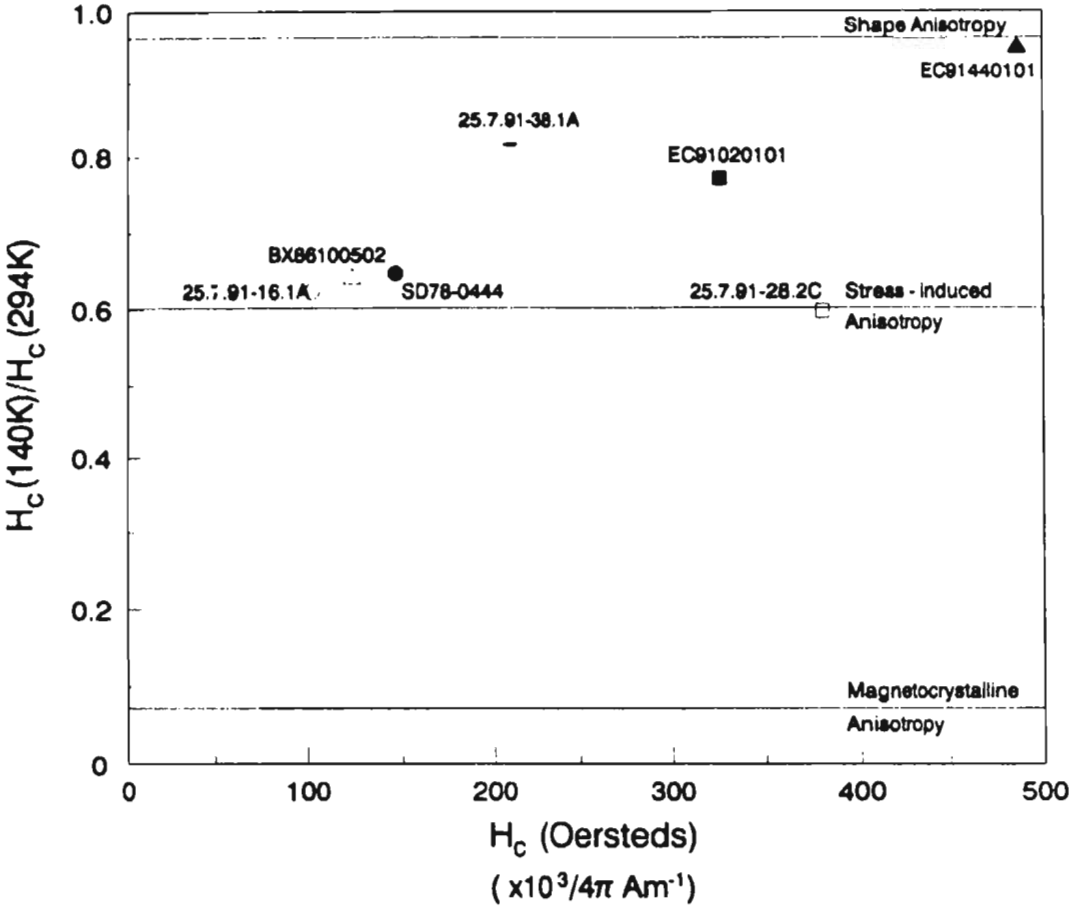

Figure 4.2: The ratio of coercive force at 140 K to that at room temperature plotted against room temperature coercive force.

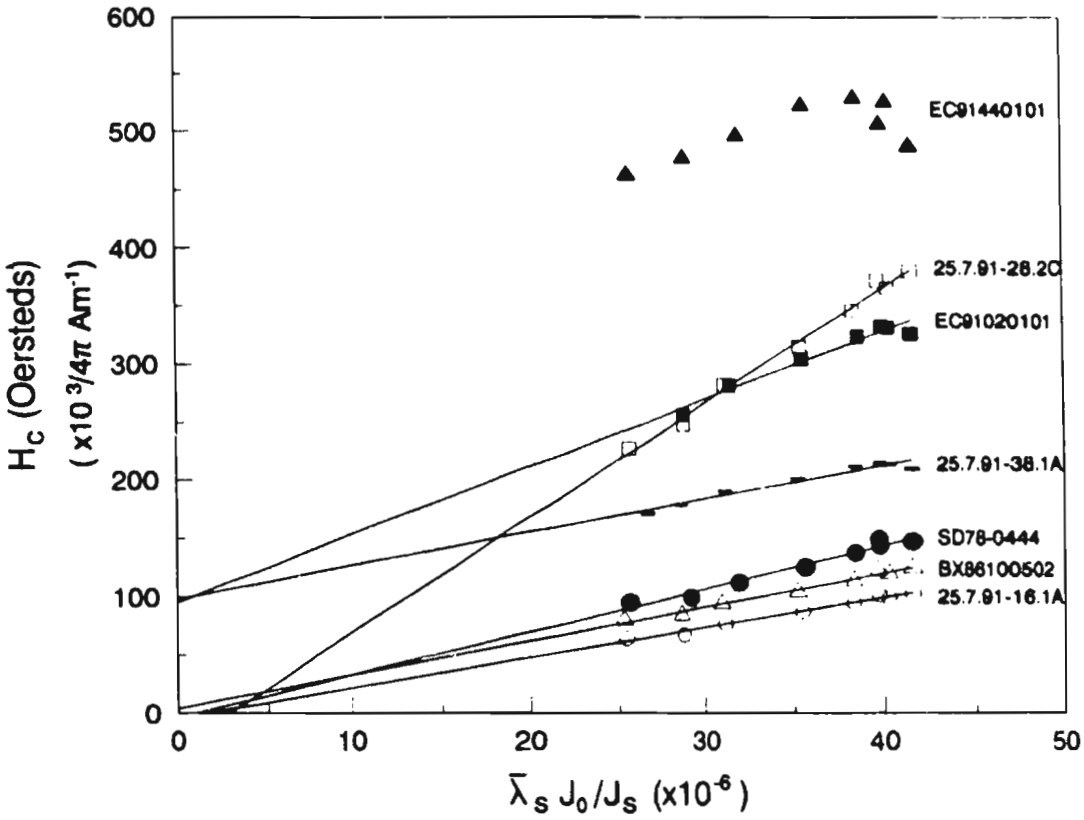

Figure 4.3: Coercive force values observed on cooling a given sample from ~300 to ~130 K plotted against the corresponding values of $\overline{\lambda}_s J_o/J_s$ for magnetite.

expected for single-domain grains dominated by shape anisotropy. However two of the lines were found to pass well above the origin perhaps because a significant fraction of their coercive force is magnetostatically controlled; these are the same two samples which suggest large contributions to coercive force from both shape anisotropy and stress-induced anisotropy in the plot in Figure 4.2.

4.3 Interpretation of J_R versus Low Temperature Results

Figure 3.9 plots saturation remanence, J_R, as a function of temperature for each of the seven rock samples. J_R was measured from the same hysteresis loops as used for H_C. Note the similar shape of both the H_C and J_R versus temperature graphs. The values of J_R decrease as the temperature is lowered from room temperature to temperatures between 128 and 118 K when a sharp increase in J_R takes place. This sudden increase is again a result of the Verwey transition at which magnetite changes its crystal structure from cubic to orthorhombic resulting in a large increase in magnetocrystalline anisotropy.

Hodych (1986b) pointed out that, for multidomain grains, we expect J_R to vary in proportion to H_C and hence in proportion to $\overline{\lambda}_S J_o/J_S$. Figure 4.4 shows the values of J_R plotted versus $\overline{\lambda}_S J_o/J_S$. The plots are linear and except for the sample of lowest coercive force, the lines all pass significantly above the origin, suggesting that the magnetite is not all multidomain. One would expect the slopes of these lines to be

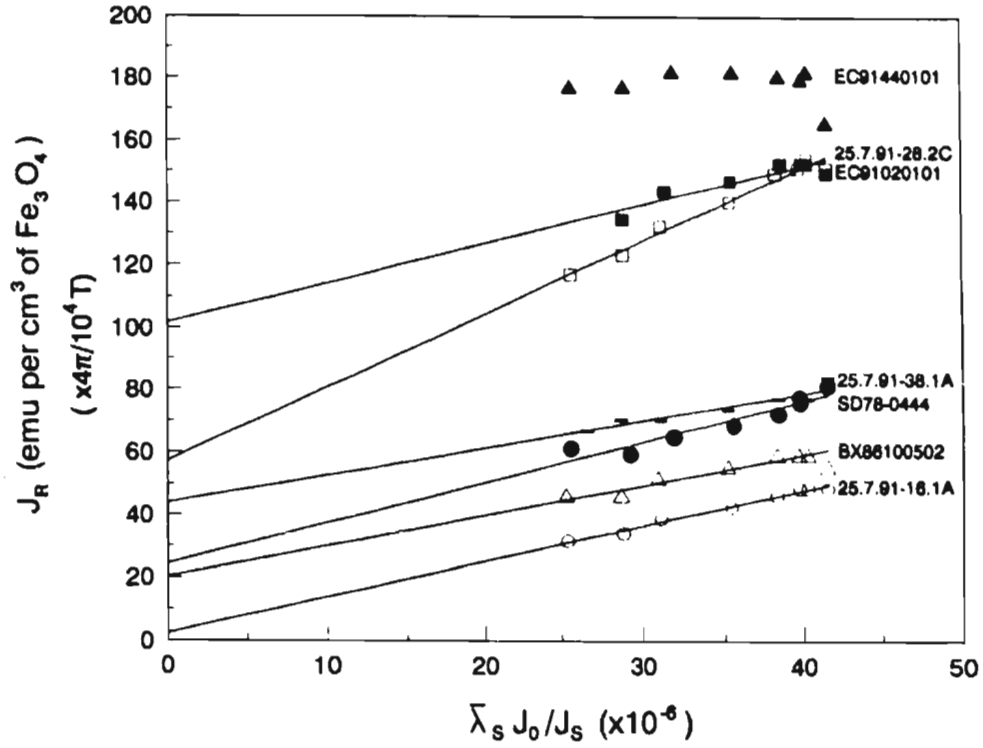

Figure 4.4: Saturation remanence values observed on cooling a given sample from ~300 to ~130 K plotted against the corresponding values of $\overline{\lambda}_S J_0/J_S$ for magnetite.

approximately 1/N of the slopes of the H_C versus $\overline{\lambda}_S J_o/J_S$ plots, if the magnetite in these samples is dominated by multidomain grains with domain wall motion magnetostrictively controlled through internal stresses (Hodych, 1990). Except for the lowest coercive force sample, the slopes are significantly less than expected, suggesting again that the magnetite is not all multidomain.

4.4 Interpretation of J_R versus H_C Plots

For multidomain grains, J_R should vary in proportion to H_C on cooling with the slope of the J_R versus H_C line equal to 1/N (Néel, 1955). The J_R versus H_C plots (Figure 4.5) are linear (except for the sample of highest coercive force whose J_R and H_C do not change much on cooling as expected of single-domain grains dominated by shape anisotropy). However, the lines often do not pass through the origin. Hodych (1990) showed theoretically that this is not explained by assuming that the dominant multidomain grains with coercive force controlled by internal stresses are accompanied by a fraction of single-domain grains with shape anisotropy. The only explanation Hodych could devise was to assume that there exists a fraction of pseudo-single-domain grains of magnetite with coercive force proportional to saturation magnetostriction as in the dominant multidomain grains, and saturation remanence proportional to saturation magnetization as in single-domain grains.

Hodych (1990) suggested a method of estimating the fractions of such

multidomain, pseudo-single-domain and single-domain grains. He assumed that a fraction f_1 of multidomain grains dominates with $H_{C1} = C_1\overline{\lambda}_S\sigma_1/J_S$ and $N_1 = H_{C1}/J_{R1}$. He also assumed a small fraction f_2 of pseudo-single-domain grains with $H_{C2} = C_2\overline{\lambda}_S\sigma_2/J_S$ and $J_{R2} = \frac{1}{2}J_S$. Finally he assumed a small fraction f_3 of single-domain grains with $H_{C3} = \frac{1}{2}(N_h - N_a)J_S$ and $J_{R3} = \frac{1}{2}J_S$. He showed that plots of J_R versus H_C, H_C versus $\overline{\lambda}_S/J_S$ and J_R versus $\overline{\lambda}_S/J_S$ on cooling should yield straight lines with slopes close to $1/N_1$, $C_1\sigma_1$ and $C_1\sigma_1/N_1$, respectively. Figure 4.6 summarizes this theory as applied by Hodych (1990) to his observations for sample SD78-0444. The J_R-intercept of J_R versus H_C should give an estimate of $\frac{1}{2}f_2(C_1\sigma_1/C_2\sigma_2)J_S$, the H_C-intercept of H_C versus $\overline{\lambda}_S/J_S$ should give an estimate of $\frac{1}{2}N_1J_S[f_2+f_3-f_2(C_1\sigma_1/C_2\sigma_2)]$ and the J_R-intercept of J_R versus $\overline{\lambda}_S/J_S$ should give an estimate of $\frac{1}{2}(f_2+f_3)J_S$. The minimum volume fraction f_2 of pseudo-single-domain grains can be estimated by taking the J_R-intercept of J_R versus H_C on cooling and dividing by $J_S/2$. The maximum f_2 can be estimated by taking the J_R-intercept of J_R versus $\overline{\lambda}_S/J_S$ on cooling and dividing it by $J_S/2$. Maximum $C_2\sigma_2$ for pseudo-single-domain grains can be estimated by taking the inverse of the J_R-intercept of J_R versus H_C on cooling and multiplying it by $C_1\sigma_1J_S/2$ and by maximum f_2. The maximum volume fraction f_3 of single-domain grains is estimated by subtracting maximum f_2 and minimum f_2.

Following Hodych (1990) Table 4.1 was made using the plots in Figures 4.3, 4.4 and 4.5. Note that the graphs in Figures 4.3 and 4.4 are of H_C and J_R versus $\overline{\lambda}_SJ_o/J_S$, making it necessary to divide the values on the x-axis by $J_o = 520$ emu/cm^3 (0.65 T) to

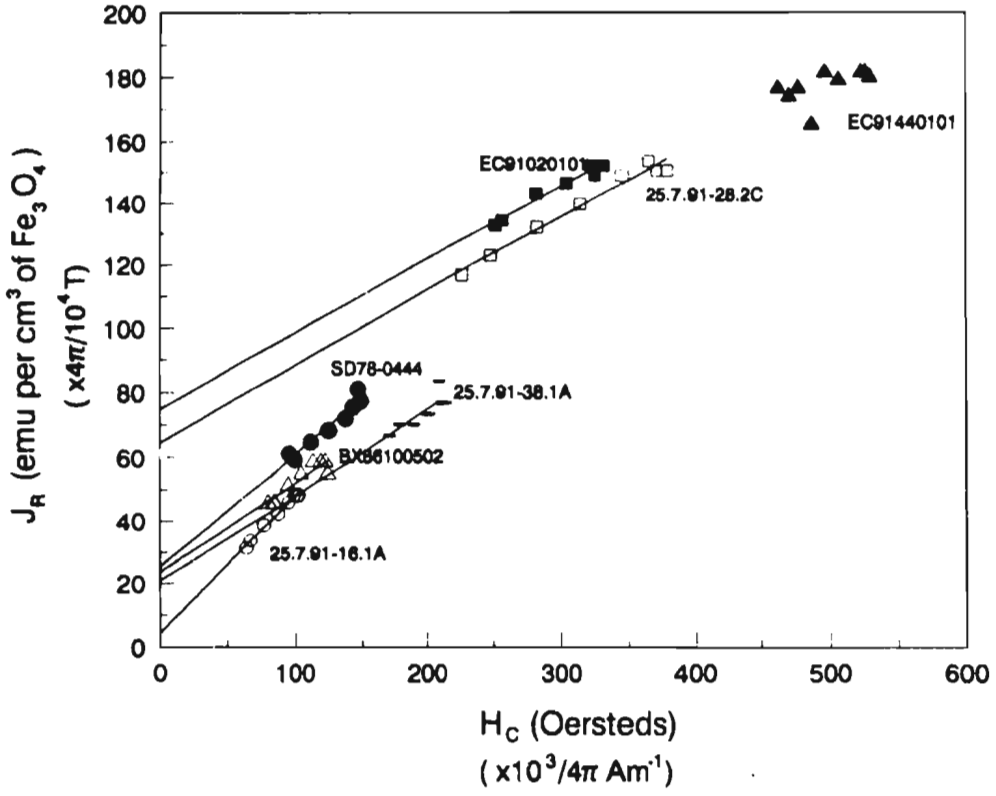

Figure 4.5: Saturation remanence J_R values observed on cooling a given sample from ~300 to ~130 K plotted against the corresponding observed coercive force H_C values.

Table 4.1: Magnetic properties

	Coercive Force	Self-demagnetizing Factor		Dominant multidomain magnetite with internal stresses σ_1	Small fraction f_2 of pseudo-single-domain grains with internal stresses σ_2			Small fraction f_3 of single-domain magnetite	Reversible Work
SAMPLE	H_C Oe ($x10^3/4\pi$ A/m)	N emu ($\div 4\pi x$ 10^{-7} H/m)	N emu ($\div 4\pi x$ 10^{-7} H/m)	$C_1\sigma_1$ ($x10^8$ dyne/cm^2) ($x10^7$ Pa)	max $C_2\sigma_2$ ($x10^8$ dyne/cm^2) ($x10^7$ Pa)	max f_2	min f_2	max f_3	$W_{rev.}$ ($x10^4$ erg/cm^3) ($x10^{-1}$ J/m^3)
25.7.91-16.1A	103	2.27	2.13	14	8	0.01	0.02	-	8.4
BX86100502	125	3.57	2.27	15	16	0.10	0.10	0.004	6.7
SD78-0444	147 (152)	2.83	1.85 (2.7)	20 (18)	19 (21)	0.10 (0.14)	0.11 (0.12)	- (0.02)	13 (26)
25.7.91-38.1A	210	3.70	2.50	14	30	0.18	0.09	0.10	5.2
EC91020101	326	4.55	2.17	29	38	0.42	0.32	0.11	5.4
25.7.91-28.2C	380	4.17	2.50	51	44	0.24	0.27	-	4.3
EC91440101	487	-	2.94	-	-	-	-	-	10

N in column 3 is estimated from the inverse slope of the plot of J_R versus H_C in Figure 4.5.
N in column 4 is estimated from the ratio of J_R/H_C from the room temperature hysteresis loops.
$C_1\sigma_1$ in column 5 is estimated from the slope of H_C versus $\lambda_S J_o J_S$ x J_o in Figure 4.3.
Max. $C_2\sigma_2$ in column 6 is estimated from the inverse of the J_R intercept of J_R versus H_C x $C_1\sigma_1 J_S^2$ x max. f_2 (Figure 4.5).
Max. f_2 in column 7 is estimated from the J_R intercept of J_R versus $\lambda_S J_o J_S \div J_S^2$ in Figure 4.4.
Min. f_2 in column 8 is estimated from the J_R intercept of J_R versus $H_C \div J_S^2$ (Figure 4.5).
Max. f_3 in column 9 is estimated from max. f_2-min. f_2.
For sample SD78-0444 the results in brackets are from Hodych (1990).

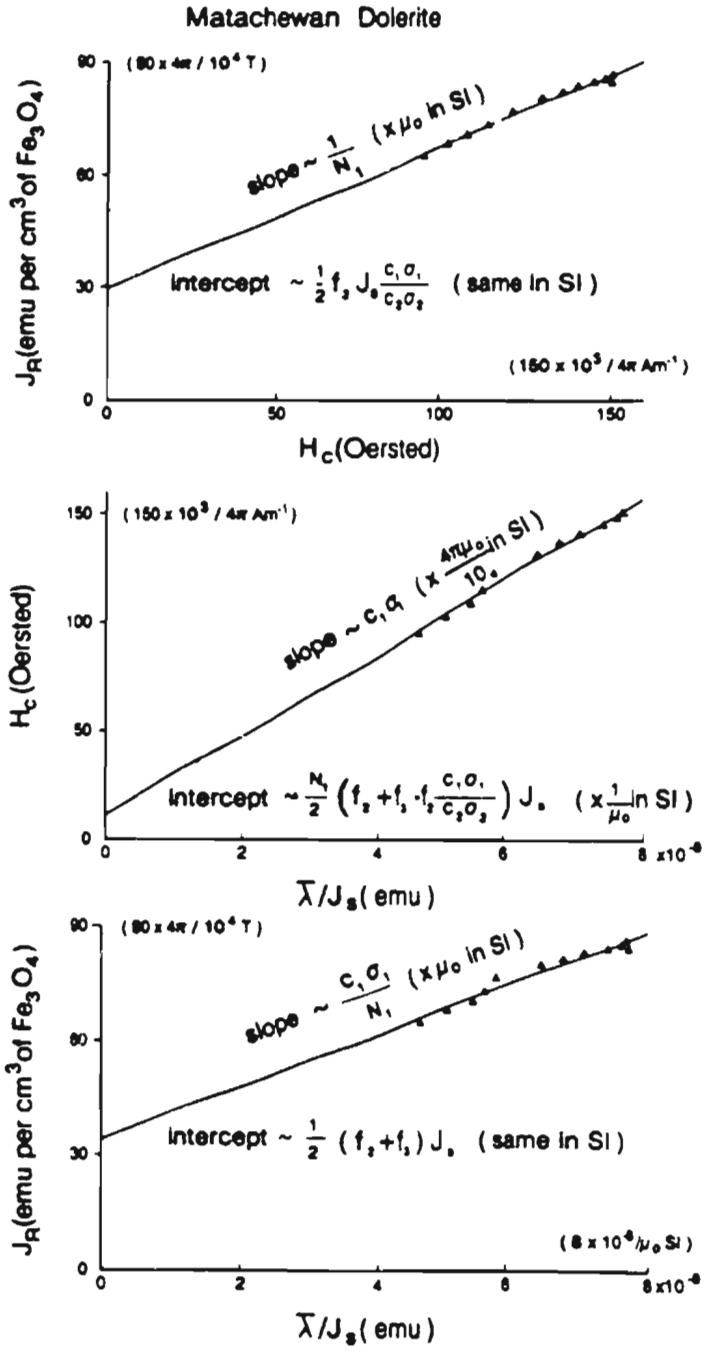

Figure 4.6: Plots that summarize the theory of Hodych (1990) applied to his measurements for the Matachewan dolerite (SD78-0444).

get the corresponding plots (Figure 4.6) of Hodych (1990).

Column 3 of Table 4.1 contains estimates of self-demagnetizing factor determined from the inverse slope of the plot of J_R versus H_C. (EC91440101 was not used because H_C and J_R did not vary enough with temperature). These N values were used to correct J_R for self-demagnetization for the J_R/J_S versus H_C plot in Figure 4.1. All the values of J_R/J_S, except for the lowest and third lowest coercive force samples significantly exceed 0.5. This suggests that most of the values for N calculated from the inverse slope of J_R versus H_C are overestimates, perhaps due to the theory breaking down when the magnetite contains more than a small fraction of pseudo-single-domain or single-domain grains. Columns 5, 6, 7, 8 and 9 of Table 4.1 follow from the theory of (Hodych, 1990) and are to be used with caution for those specimens in which N was overestimated.

Column 4 of Table 4.1 contains values of N estimated from the ratio of H_C/J_R. All of the N values calculated in this manner were lower than those found using the inverse slope of the J_R versus H_C plot, and agree more closely with the theories of Dunlop (1983) and Davis and Evans (1976) who estimate values of N between ~1.6 and ~2.0 emu (~1.3×10^6 and 1.6×10^6 H/m).

Note that the hysteresis loops to 3600 Oe (360 mT) of this thesis give very similar results and predictions as the hysteresis loops to 1200 Oe (120 mT) of Hodych (1990) for the Matachewan dolerite sample (SD78-0444). The results of Hodych (1990) are given in brackets below the results of this thesis in Table 4.1. (His result for W_{rc}

is also given and is higher than mine because it is for the 6000 Oe (600 mT) loop of Figure 4.7).

Column 5 of Table 4.1 is an estimate of $C_1\sigma_1$ calculated from the slope of H_C versus $\overline{\lambda}_S J_o/J_S \times J_o$ where σ_1 is the internal stress magnitude of the dominant multidomain grains and where C_1 can have a maximum value of approximately 4 according to the theory of Chikazumi (1964). Minimum internal stress ($C_1\sigma_1/4$) is estimated to be 6×10^8 dyne/cm^2 (6×10^7 Pa) on average. For comparison, the breaking stress of gabbro under compression is 18×10^8 dyne/cm^2 (18×10^7 Pa) according to Jaeger (1956).

Column 6 of Table 4.1 is an estimate of the maximum $C_2\sigma_2$, where σ_2 is the internal stress in the pseudo-single-domain grains forming a fraction f_2 of the magnetite in the samples. These values were calculated from the inverse of the J_R intercept of J_R versus $H_C \times C_1\sigma_1 J_S/2 \times \max.f_2$. The average value of the maximum $C_2\sigma_2$ was approximately 26×10^8 dynes/cm^2 (26×10^7 Pa) but is not as useful as $C_1\sigma_1$ since the value of C_2 is not known.

Columns 7 and 8 of Table 4.1 are estimates of the maximum and the minimum fraction f_2 of pseudo-single-domain grains that have H_C controlled by $\overline{\lambda}_S$ but have J_R controlled by J_S. The maximum fraction f_2 was calculated from the J_R intercept of $\overline{\lambda}_S J_o/J_S \div J_S/2$, and the minimum fraction f_2 was calculated from the J_R intercept of J_R versus $H_C \div J_S/2$. The average value of maximum f_2 was 0.18, and the average value of minimum f_2 was 0.15.

Column 9 of Table 4.1 is the maximum fraction f_3 of single-domain grains of

magnetite in the samples, calculated from maximum f_2 - minimum f_2. This column suggests a very small fraction of single-domain grains (less than 10% even for the higher coercive force samples). However the highest coercive force sample could not be analyzed in this way because neither H_C nor J_R change significantly on cooling and because it is likely dominated by single-domain grains whereas the analysis assumes only a small fraction of single-domain grains.

4.5 Interpretation of Reversible Work versus Low Temperature Results

In the absence of self-demagnetizing fields, reversible work, W_{rev}, recovered between saturation and the remanence point of the sample's hysteresis loop is defined by Bozorth (1951) as:

$$W_{rev} = \int_{J_R}^{J_S} H dJ$$

In the presence of self-demagnetizing fields, W_{rev} can be estimated by measuring the area shown dotted in Figure 4.7 from Hodych (1990).

Appel (1987) following a 1932 paper by Kersten (*discussed in* Bozorth, 1951) assumed that internal stresses σ could be estimated from $W_{rev} = \lambda_s \sigma$. Hodych (1990) argued that, if W_{rev} were mainly due to anisotropy induced by internal stresses, W_{rev}

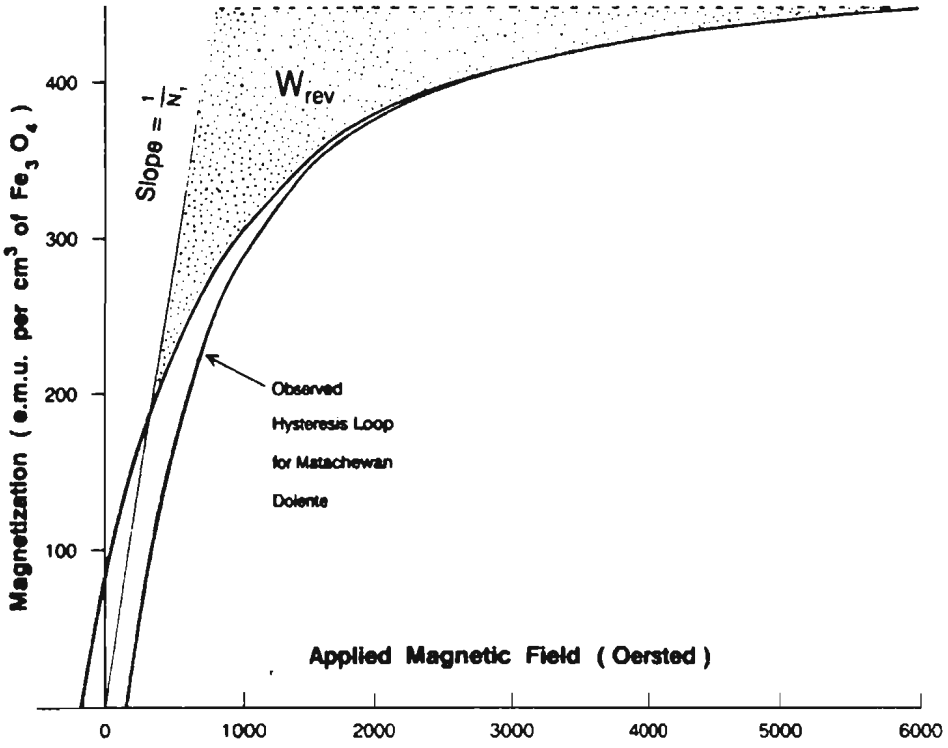

Figure 4.7: Area measured to estimate W_{rev} (=26x10^4 erg per cm^3 of magnetite) from Hodych (1990) using hysteresis loop to 6000 Oe (600 mT) for sample SD78-0444.

should decrease in proportion to $\overline{\lambda}_S$ on cooling to approximately 120 K. Hodych (1990) attempted to measure the change W_{rev} on cooling for various magnetite bearing rock samples using hysteresis loops plotted to 1200 Oe (120 mT). The reversible work recovered between near-saturation and the remanence point, in the absence of demagnetizing fields, was estimated by measuring the area (dotted in Figure 4.7) bounded by the descending arm of the hysteresis loop, the line of slope 1/N and a horizontal line drawn through J at 1200 Oe (120 mT). Hodych (1990) found that W_{rev} was approximately independent of temperature for all his samples. This suggested that rotation against magnetostatic rather than magnetostrictive or magnetocrystalline forces might mostly be responsible for W_{rev} in his samples since magnetostatic forces are proportional to J_S, which changes little on cooling. Hence it seemed unlikely that W_{rev} could give an estimate of internal stress magnitude in his samples.

Figure 4.8 shows the procedure of Hodych (1990) repeated to higher field 3600 Oe (360 mT), on the Matachewan dolerite (SD78-0444) which was one of the specimens used by Hodych. Again, W_{rev} is found to show little variation on cooling to approximately 125 K. (The same is true of the rest of the samples as can be seen in Figure 3.12) Also, Figure 4.8 shows that the lack of variation of W_{rev} on cooling does not depend on the field strength chosen for the integration, for fields from 1100 to 3600 Oe (110 to 360 mT).

Note, however, that W_{rev} is defined as an integration with respect to magnetization rather than field. Hence, it would seem more valid to measure W_{rev} to a

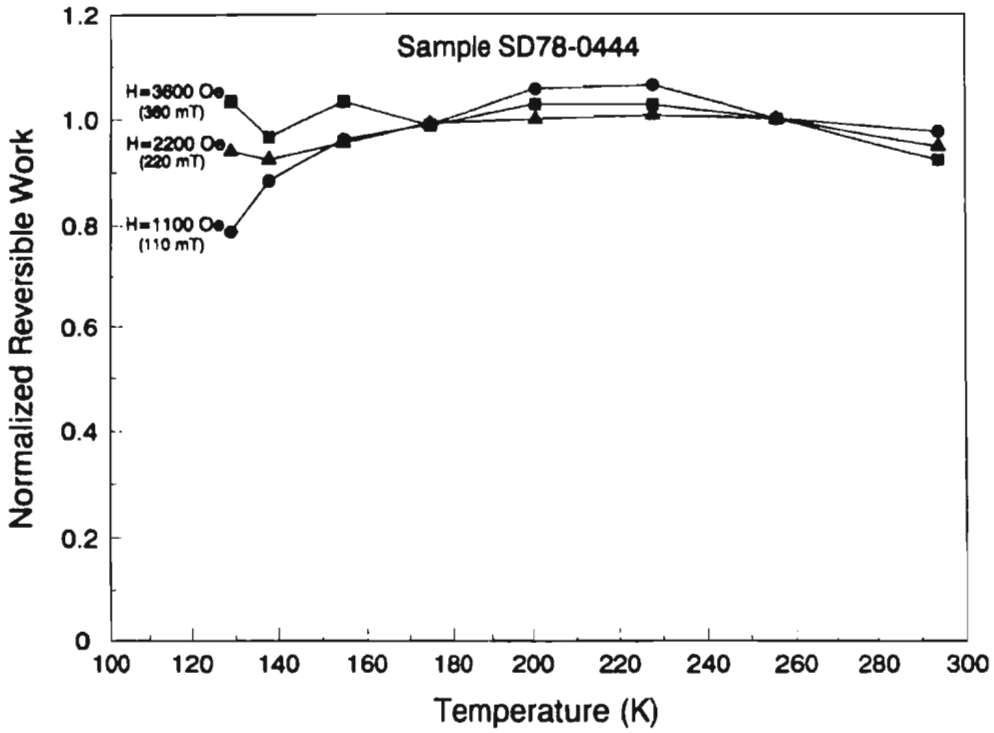

Figure 4.8: Normalized reversible work (integrating to the various constant fields indicated) versus temperature.

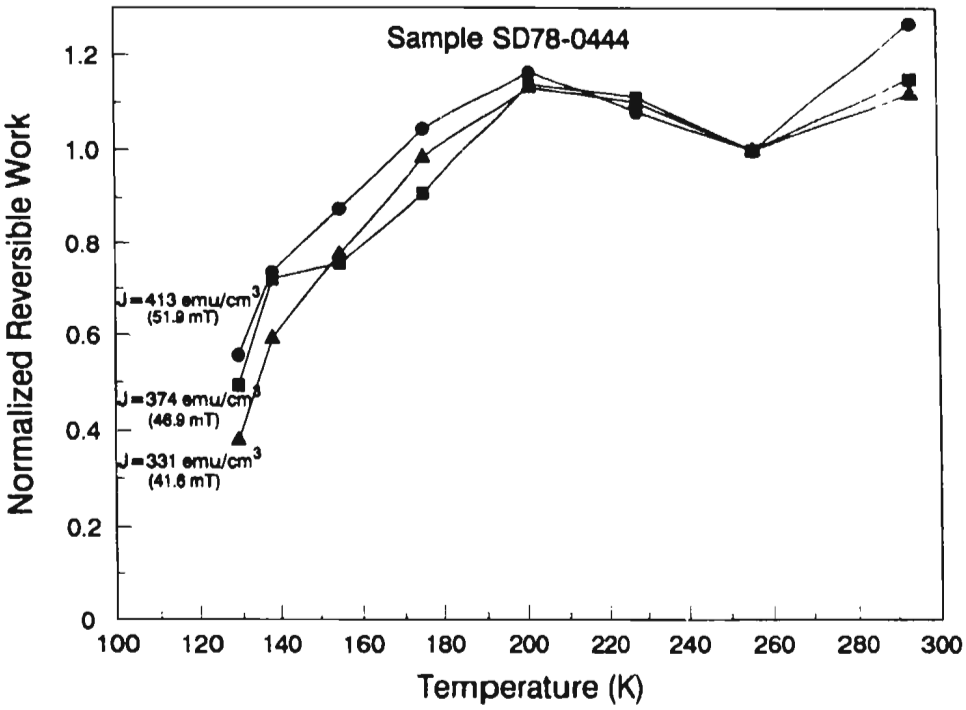

Figure 4.9: Normalized reversible work (integrating to the various constant magnetizations indicated) versus temperature.

constant magnetization value rather than to a constant field value. This was done for the Matachewan dolerite sample (SD78-0444) and is plotted in Figure 4.9. Note that instead of W_{rev} remaining about constant on cooling, W_{rev} decreases on cooling roughly like $\overline{\lambda}_S$ as expected if domain rotation was opposed by stress-induced anisotropy. Also Figure 4.9 shows that W_{rev} decreasing on cooling like $\overline{\lambda}_S$ does not depend on the constant magnetization value chosen for the integration (for magnetizations between 331 and 413 emu per cm^3 of magnetite in the sample (41.6 - 51.9 mT))

Both methods of evaluating W_{rev} should have given the same result if the samples had saturated by 3600 Oe (360 mT). However, saturation magnetization (J_S) has not been reached by 3600 Oe (360 mT) in the Matachewan dolerite (Figure 3.1) or any of the other samples (Figures 3.5 to 3.7). Figure 4.10 is a plot of W_{rev} (integrated to a constant field) versus the strength of the field to which W_{rev} was integrated. The figure shows that W_{rev} is increasing as a linear function of the field to which W_{rev} is integrated. W_{rev} is not even beginning to saturate at the highest field used (3600 Oe (360 mT)) even though this is a sample with one of the lower H_C values and hence should be one of the easier samples to saturate. This remains true at lower temperatures (201 and 129 K). It seems that my estimate of W_{rev} may grossly underestimate the saturation value of W_{rev} whether integrated to constant field or constant magnetization.

However, the shape of the W_{rev} (integrated to constant magnetization) versus temperature plot remains the same whether one integrates to the highest magnetization attained or to a lower magnetization, as seen in Figure 4.9. This gives some hope that

the shape of the W_{rev} versus temperature plots integrated to constant magnetization may possibly be used to infer what is controlling domain rotation (domain wall motion is expected to make a relatively small contribution to W_{rev}). W_{rev} versus temperature estimates (integrated to constant magnetization) were normalized and plotted on the same graph as normalized values of J_S, $\overline{\lambda}_S$ and K_1 plotted versus temperature (Figure 4.11). The highest coercive force sample did not give useable results because the hysteresis loops drawn at the lower temperatures were very noisy, making it impossible to determine accurate reversible work values. Column 10 of Table 4.1 lists the room temperature values of W_{rev}. The normalized W_{rev} versus temperature plots do not resemble nor do they fall between the normalized J_S, $\overline{\lambda}_S$ or K_1 versus temperature plots. This suggests that these W_{rev} versus temperature plots cannot be used to infer what is controlling domain rotation in these samples. The one possible exception is the Matachewan dolerite (SD78-0444) whose W_{rev} versus temperature plot roughly resembles that of $\overline{\lambda}_S$ versus temperature suggesting that stress may possibly control its domain rotation. However, this resemblance may be fortuitous. In general, we do not believe that W_{rev} can be used to identify what controls domain rotation or to estimate internal stresses in the specimens studied for this thesis.

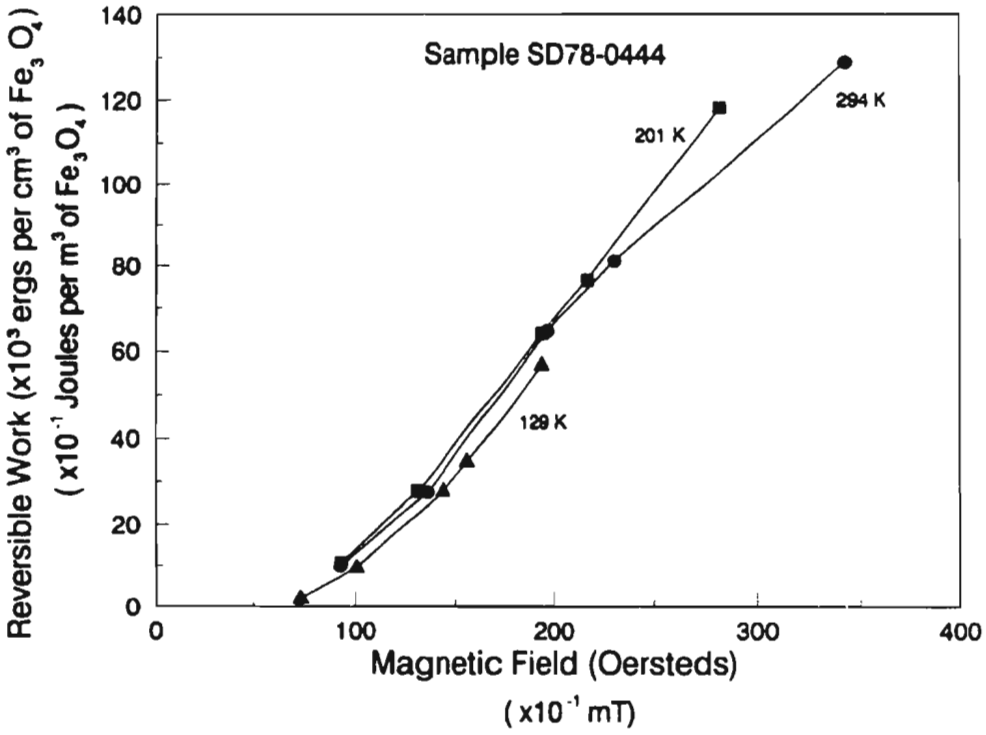

Figure 4.10: Reversible work W_{rev} (integrating to constant field) versus strength of magnetic field to which W_{rev} is integrated.

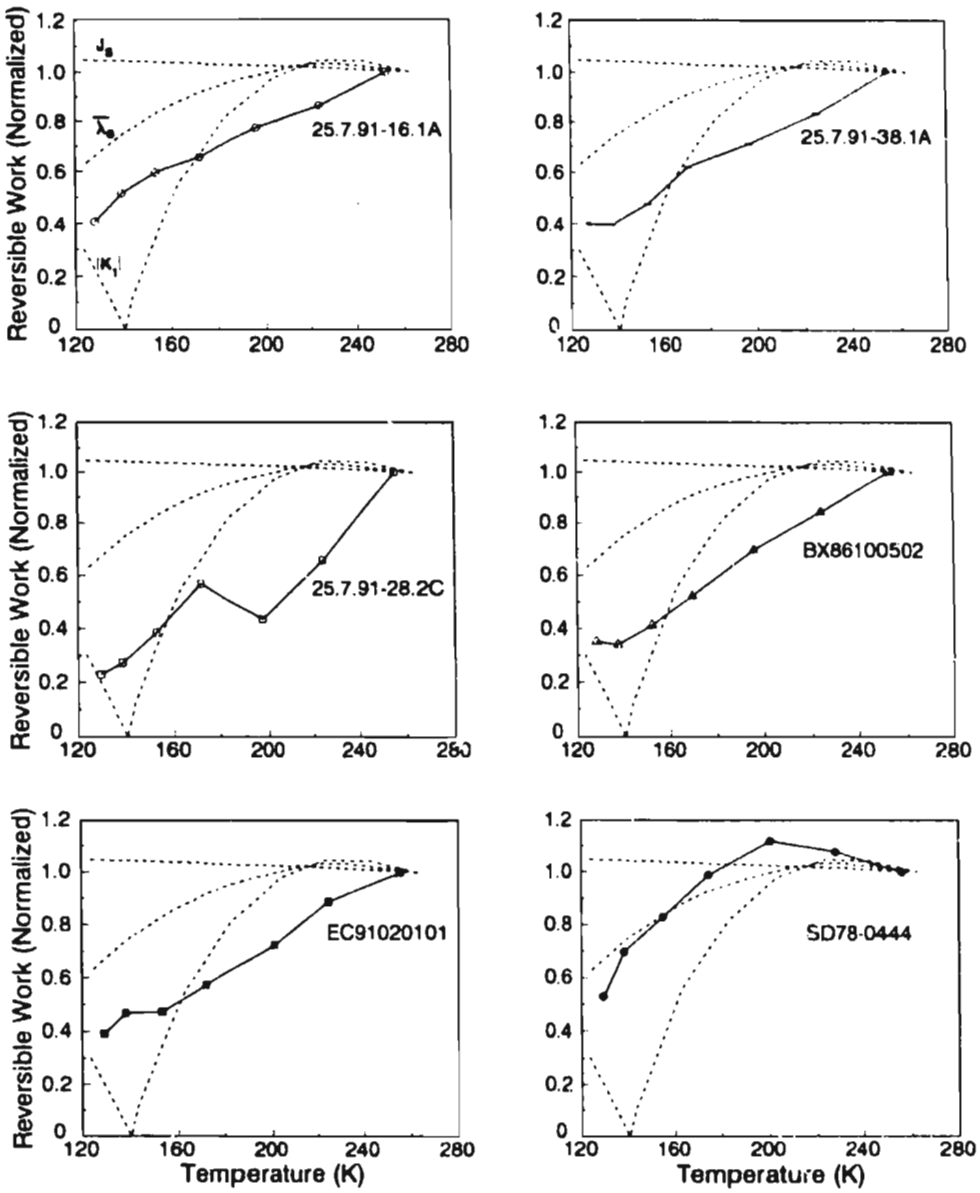

Figure 4.11: Normalized reversible work (integrating to constant magnetization) versus temperature.

4.6 Summary

Seven Precambrian dolerite samples, with a remanence that is likely primary, were selected for study in the new vibrating-sample magnetometer. They were chosen because of their high magnetite content (a few percent) and their high coercive force values ranging from 103 to 487 Oe (8.2×10^3 A/m to 3.9×10^4 A/m). Hysteresis loops to 3600 Oe (360 mT) were plotted for various temperatures from room temperature to near liquid nitrogen temperature for each of these samples. Values of coercive force, H_C, saturation remanence, J_R and reversible work, W_{rev} were measured from the hysteresis loops and plotted against decreasing temperature.

H_C varied as a linear function of $\overline{\lambda}_S J_o/J_S$ on cooling to approximately 120 K, as expected from the theory of Néel (1946) if H_C is mainly magnetostrictively controlled through internal stresses opposing domain wall motion. The one exception was the highest coercive force sample whose H_C was almost invariant on cooling to ~120 K, as expected of single-domain grains with H_C controlled by shape anisotropy. Between about 128 and 118 K, H_C increased due to the Verwey transition at which magnetite changes its crystal structure from cubic to orthorhombic resulting in a large increase in magnetocrystalline anisotropy.

J_R decreased on cooling similarly to H_C and also showed a Verwey transition between about 128 and 118 K. The plots of J_R versus $\overline{\lambda}_S J_o/J_S$ were linear on cooling as expected of grains in which H_C is mainly magnetostrictively controlled by internal

stresses opposing domain wall motion. The main exception again was the highest coercive force sample whose J_R was almost invariant on cooling to approximately 120 K as expected of H_C controlled by shape anisotropy.

The plots of J_R versus H_C on cooling were linear (except for the highest coercive force sample in which neither J_R nor H_C changed much on cooling). However, the lines mostly pass well above the origin. This can be explained (Hodych, 1990) by assuming that a small fraction of magnetite exists in pseudo-single-domain grains whose coercive force is magnetostrictively controlled as in the dominant multidomain grains, but whose saturation remanence is $\frac{1}{2}J_S$ as in single-domain grains.

Following Hodych (1990), estimates were made of the minimum value of the internal stresses, σ_i, of the dominant multidomain grains. The magnitude of these stresses averaged 6×10^8 dyne/cm^2 (6×10^7 Pa) which is less than the 18×10^8 dyne/cm^2 (18×10^7 Pa) breaking stress of gabbro in compression.

When estimated by integrating to a constant field, W_{rev} showed little variation on cooling (agreeing with the findings of Hodych (1990)). However, it should be more valid to estimate W_{rev} by integrating to a constant magnetization. When this was done, W_{rev} was found to decrease on cooling. Unfortunately, the plot of W_{rev} versus temperature does not resemble nor does it fall between the plots of $\overline{\lambda}_S$, $|K_1|$ or J_S versus temperature (except perhaps for the Matachewan dolerite sample). Hence we do not believe that W_{rev} versus temperature plots can be used to infer what controls domain rotation in the samples studied.

BIBLIOGRAPHY

Appel, E., 1987. Stress anisotropy in Ti-rich titanomagnetites. Physics of the Earth and Planetary Interiors, 46, pp. 233-240.

Argyle, K.S. and Dunlop, D.J., 1990. Low-temperature and high-temperature hysteresis of small multidomain magnetites (215-540 nm). Journal of Geophysical Research, Vol. 95, No. B5, pp. 7069-7083.

Bickford, L.R., Pappis, J. and Stull, J.L., 1955. Magnetostriction and permeability of magnetite and cobalt-substituted magnetite. Physical Review, 99, pp. 1210-1214.

Blackett, P.M.S. and Sutton, P., 1956. Lectures in Rock Magnetism. Weizmann Science Press, Jerusalem.

Butler, R.F., 1992. Palaeomagnetism. Blackwell, Boston, 319 pp.

Buchan, K.L. and Halls, H.C., 1990. Palaeomagnetism of Proterozoic mafic dyke swarms of the Canadian Shield *in* Mafic Dykes and Emplacement Mechanisms. Eds. Parker, A.J., Rickwood, P.C. and Tucker, D.H., Balkema, Rotterdam.

Bozorth, R.M., 1951. Ferromagnetism. Van Nostrand, New York, 968 pp.

Carmichael, R.S., 1989. Practical Handbook of Physical Properties of Rocks and Minerals. Ed. R.S. Carmichael, CRC Press, Boca Raton, Florida, 741 pp.

Chikazumi, S., 1964 Physics of Magnetism. Wiley, New York, 554 pp.

Creer, K.M., De Sa, A. and O'Reilly, W., 1967. New vibrating-sample magnetometers for use between 4 and 1000 K. Journal of Scientific Instruments, 44, pp. 133-135.

Cullity, B.D., 1972. Introduction to Magnetic Minerals. Addison-Wesley, Reading, MA, 666 pp.

Davis, P.M. and Evans, M.E., 1976. Interacting single-domain properties of magnetic intergrowths. Journal of Geophysical Research, 81, pp. 989-994.

Day, R., Fuller, M. and Schmidt, V.A., 1977. Hysteresis properties of titanomagnetites: grain-size and compositional dependence. Physics of the Earth and Planetary Interiors, 13, pp. 260-267.

Deutsch, E.R. and Pätzold, R.R., 1976. Magnetism of basalt cores from the Nazca Plate and implications for magnetic anomaly interpretation. Journal of Geophysical Research, 81, pp. 4188-4198.

Dunlop, D.J., 1981. The rock magnetism of fine particles. Physics of the Earth and Planetary Interiors, 26, pp. 1-26.

Flanders, P.J., 1967. The rotating-sample magnetometer. Journal of Applied Physics, 38, pp. 1293-1294.

Flanders, P.J., 1988. An alternating gradient magnetometer. Journal of Applied Physics, 63, pp. 3940-3945.

Foner, S., 1959. Versatile and sensitive vibrating-sample magnetometer. The Review of Scientific Instruments, 30, pp. 548-557.

Fuller, M., 1987. Methods of Experimental Physics. Academic Press Inc., Vol. 24, Part A, pp. 303-477.

Hodych, J.P., 1982a. Magnetostrictive control of coercive force in multidomain magnetite. Nature, 298, pp. 542-544.

Hodych, J.P., 1982b. Magnetic hysteresis as a function of low temperature for deep-sea basalts containing large titanomagnetite grains - inference of domain state and controls on coercivity. Canadian Journal of Earth Sciences, 19, pp. 144-152.

Hodych, J.P., 1986a. Determination of self-demagnetizing factor N for multidomain magnetite grains in rock. Physics of the Earth and Planetary Interiors, 41, pp. 283-291.

Hodych, J.P., 1986b. Evidence for magnetostrictive control of intrinsic susceptibility and coercive force of multidomain magnetite in rocks. Physics of the Earth and Planetary Interiors, 42, pp. 184-194.

Hodych, J.P., 1990. Magnetic hysteresis as a function of low temperature in rocks: evidence for internal stress control of remanence in multidomain and pseudo-single-domain magnetite. Physics of the Earth and Planetary Interiors, 64, pp. 21-36.

Hodych, J.P., 1991. Low-temperature demagnetization of saturation remanence in rocks bearing multidomain magnetite. Physics of the Earth and Planetary Interiors, 66 pp. 144-152.

Jaeger, J.C., 1956. Elasticity Fracture and Flow. Methuen, New York, 152 pp.

Kobayashi, K. and Fuller, M., 1967. *in* Methods in Palaeomagnetism. Ed. D.W. Collinson, K.M. Creer, S.K. Runcorn, Elsevier, Amsterdam, pp. 450-456.

Morrish, A.H. and Watt, L.A.K., 1958. Coercive force of iron oxide micropowders at low temperatures. Journal of Applied Physics, Vol. 9, No. 7, pp. 1029-1033

Murthy, G.S., Deutsch, E.R. and Pätzold, R.R., 1976. Inferences on the magnetic domain state of ieg 37 basalts. Journal of Geophysical Research, 81, pp. 4199-4206.

Néel, L., 1946. Bases d'une nouvelle théorie générale du champ coercitif. Annales, Université de Grenoble, 22, pp. 299-343.

Néel, L., 1955. Some theoretical aspects of rock magnetism. Advances in Physics, 4, pp. 191-243.

Pauthenet, R., 1950. Variation thermique de l'aimanation spontanée des ferrites de nickel, cobalt, fer et manganése. Comptes Rendues Academie Science Paris, 230, pp. 1842-1843.

Payne, M.A., 1981. SI and gaussian cgs units, conversions and equations for use in geomagnetism. Physics of the Earth and Planetary Interiors, 26, pp. 2-12.

Radhakrishnamurty, C., Raja, P.K.S., Likhite, S.D. and Sahasrabudhe, P.W., 1972. Problems concerning the magnetic behaviour and determination of Curie points of certain basalts. Pure and Applied Geophysics, 93, pp. 129-140.

Radhakrishnamurty, C., Likhite, S.D., Deutsch, E.R. and Murthy, G.S., 1978. Nature of magnetic grains in basalts and implications for palaeomagnetism. Proceedings of the Indian Academy of Science, Section A, 87, pp. 235-243.

Schmidbauer, E. and Schembera, N., 1987. Magnetic hysteresis properties and anhysteretic remanent magnetization of spherical Fe_3O_4 particles in the grain size range 60-160 nm. Physics of the Earth and Planetary Interiors, 46, pp. 77-83.

Shive, P.N., 1986. Suggestions for the use of SI units in magnetism. EOS, 67, p. 25.

Stewart, K.H., 1954. Ferromagnetic Domains. Cambridge University Press, 176 pp.

Stoner, E.C. and Wolfarth, E.P., 1948. A mechanism of magnetic hysteresis in heterogeneous alloys. Philosophical Transactions of the Royal Society London Series A, 240, pp. 599-642.

Syono, Y., 1965. Magnetocrystalline anisotropy and magnetostriction of Fe_3O_4-Fe_2TiO_4 series with special application to rock magnetism. Japanese Journal of Geophysics, 4, pp. 71-143.

Worm, H.-U. and Markert, H., 1987. Magnetic hysteresis properties of fine particle titanomagnetites precipitated in a silicate matrix. Physics of the Earth and Planetary Interiors, 46, pp. 84-92.

Xu, S. and Merrill, R.T., 1989. Microstress and microcoercivity in multidomain grains. Journal of Geophysical Research, 94B, pp. 10627-10636.

Xu, S. and Merrill, R.T., 1990. Microcoercivity, bulk coercivity and saturation remanence in multidomain grains. Journal of Geophysical Research, Vol. 95, No. B5, pp. 7083-7090.